Targeting Lysosomal pH Restores Mitochondrial Quality Control in GBA1-Mutant Parkinson's Disease

Preethi Sheshadri[1,†],

Maria Alicia Costa Besada[1,#],

Alessia Fisher[1],

Szilvia Kiraly[2],

Kritarth Singh[1],

Ioanna Kourouzidou[1,‡],

Thomas S. Blacker[3]

Jialiu Zeng[5]

Orian S Shirihai[4],

Mark W Grinstaff[5],

Michael R Duchen[1,*].

1- University College London, Department of Cell and Developmental Biology, WC1E 6BT and UCL Consortium for Mitochondrial Research. .
2- UCL Institute of Ophthalmology, Bath Street, London EC1V9EL.
3- UCL, Department of Structural and Molecular Biology, London, WC1E 6BT.
4- Department of Medicine, David Geffen School of Medicine, University of California, Los Angeles, CA 90095.
5- Departments of Biomedical Engineering and Chemistry, Boston University, MA 02215.

* - Correspondence to Michael R. Duchen; email – m.duchen@ucl.ac.uk
† - Current address - UK Dementia Research Institute, Cardiff University, CF24 4HQ.
# - Current address - Research Center for Molecular Medicine and Chronic Diseases (CIMUS), Research Health Institute of Santiago (IDIS), University of Santiago de Compostela, Santiago de Compostela, Spain. Networking Research Center on Neurodegenerative Diseases (CIBERNED), Madrid, Spain.
‡ - Current address - Biofabrics, Rua do Campo Lindo, Porto, Portugal.

Abstract

Heterozygous mutations in the Glucocerebrosidase gene (*GBA1*), encoding the lysosomal hydrolase β-glucocerebrosidase (GCase), are a genetic risk factor for Parkinson's disease (PD). To explore the pathophysiological consequences of these mutations, we have used fibroblasts and dopaminergic neurons generated from induced pluripotent stem cells (iPSCs) derived from patients with *GBA1* related PD. GCase activity, lysosomal acidification, protease activity, mitophagy and mitochondrial bioenergetic function were all impaired. Mitochondria were fragmented, with reduced membrane potential and oxygen consumption. We propose that impaired bioenergetic function is a consequence of impaired lysosomal acidification and compromised mitophagy. The V-ATPase complex drives lysosomal acidification. Its assembly is regulated by MTORC1, which is constitutively phosphorylated in mutant cells. FLIM-FRET measurements confirmed impaired V-ATPase assembly which reversed following rapamycin treatment. Acidic nanoparticles, which accumulate in lysosomes, rescued lysosomal pH, and restored mitophagy and mitochondrial membrane potential in *GBA1* mutant dopaminergic neurons. These data identify a core pathway as a potential therapeutic target for the treatment of *GBA1*-mediated Parkinson's Disease. (160 words)

Keywords: GBA1, mitochondria, lysosomes, lysosomal pH, MTOR, acidic nanoparticles

Introduction

Genome-wide association studies have revealed that mutations of the glucocerebrosidase (*GBA1*) gene constitute a significant risk factor in the development of Parkinson's Disease (PD)[60]. The *GBA1* gene encodes the enzyme β-glucocerebrosidase (GCase), which generates glucose and ceramide from glucosylceramide within lysosomes. While homozygous *GBA1* mutations cause Gaucher Disease, which may include a significant neurodegenerative component[23], heterozygous mutations are associated with an increased risk of developing PD. The two most prevalent *GBA1* mutations associated with PD are the N370S and L444P mutations[39]. Intriguingly, the less common E326K mutation in *GBA1* exhibits a relatively mild effect on GCase activity, does not cause Gaucher's Disease, but is correlated with PD risk[18].

Mitochondrial dysfunction appears to constitute a defining characteristic of PD[28]. The adverse impact of dysfunctional mitochondrial oxidative phosphorylation (OXPHOS) on the viability of dopaminergic (DA) neurons is substantiated by experimental models of PD that result from toxins that target complex I[28]. The *Gba1* mouse knockout model, a model of severe neurodegeneration, exhibited severe mitochondrial dysfunction in primary neurons and astrocytes in culture, alongside neurological pathologies associated with PD, including disruption of autophagy-lysosomal pathways, and the accumulation of ubiquitinated proteins and α-synuclein[49].

The autophagosome-lysosome axis and ubiquitin proteasome systems accomplish degradation of dysfunctional organelles and protein degradation and together play a critical role in cellular quality control[34]. Lysosomal acidification generating pH values between 4.5 to 4.7[52] is essential for normal lysosomal function and is required for the activity of lysosomal hydrolytic enzymes and effective protein degradation[44,12]. The acidification is generated by the vacuolar-type H^+ ATPase (V-ATPase), a proton pump composed of a peripheral V_1 domain, which hydrolyses ATP, and a membrane-integrated V_o domain, responsible for the translocation of protons into the lysosomal lumen[17]. Disrupted V-ATPase assembly and V-ATPase dysfunction have been reported associated with multiple disorders[20], including Juvenile-onset Parkinson's Disease[55], Alzheimer's Disease[8, 70], Epilepsy[21, 26] and Down's syndrome[30].

GBA1-linked pathologies such as Gaucher's disease and PD are associated with a dysfunctional autophagy-lysosome pathway, including impaired lysosomal regeneration from autolysosomes during macroautophagy[58,59]. These investigations suggest that targeting the dysfunctional lysosomal system and the autophagy-lysosome pathway may serve as a potential therapeutic strategy for PD linked to *GBA1* mutations. Although numerous studies indicate that impaired lysosomal acidification plays a role in neuronal pathologies associated with various neurodegenerative disorders[38] and that GBA1-PD is characterised by lysosomal dysfunction [44], the effects of compromised lysosomal acidification in GBA1-PD have not been extensively examined.

In this study, we have characterised the consequences of *GBA1* mutations associated with PD for mitochondrial and lysosomal function in patient-derived fibroblasts and DA neurons

generated from patient-derived induced pluripotent stem cells (iPSC). As GBA1 is a lysosomal enzyme, we hypothesised that lysosomal dysfunction as a consequence of the mutations, might lead to impaired mitochondrial function, initiating a pathophysiological cascade culminating in cell injury. Furthermore, we found that constitutive and inappropriate activation of mechanistic target of rapamycin complex 1 (MTORC1) contributes to impaired lysosomal acidification through aberrant assembly of the V-ATPase complex, leading to lysosomal dysfunction. Additionally, we demonstrate that the restoration of lysosomal pH ameliorates autophagy and rescues both lysosomal and mitochondrial function in cells carrying GBA1-PD mutations.

Results

To characterise the impact of PD-related *GBA1* mutations on lysosomal and mitochondrial function, we examined three lines of human dermal fibroblasts and six iPSC lines derived from GBA1-PD patients carrying E326K or N370S mutations, along with two healthy controls. We also included one CRISPR-corrected isogenic control iPSC line each for GBA1-N370S and GBA1-E326K iPSCs. (Table 1).

Lysosomal function is impaired in cells with PD-related GBA1 mutations

As GBA1 is a lysosomal enzyme, our investigation began by characterising the lysosomes in fibroblasts and DA neurons from both control and PD patient-derived iPSCs. The GBA1 protein expression levels measured by western blot were not significantly different between the control and *GBA1* mutant neurons; however, GCase enzymatic activity was significantly reduced in iPSC-DA neurons and fibroblasts carrying either *GBA1* mutation (Fig 1A, B, S1A, B). Lysosomal acidification was measured using the ratiometric pH-sensitive dye, Lysosensor Yellow/Blue DND160. These data revealed impaired acidification in both E326K and N370S DA neurons and fibroblasts (Fig 1C, S1C, D). Calibration of the lysosomal pH (see methods) gave values of 4.74±0.03 - 4.77±0.02 in control cells but between 4.89±0.02 and 5.06±0.03 in the mutant fibroblasts (Fig 1D). The function of endocytic trafficking and lysosomal proteolytic activity was measured using the DQ-Red BSA assay. DQ-Red BSA intensity was significantly reduced in the *GBA1* mutant neurons, indicating impaired lysosomal degradative function in GBA1-PD cells (Fig 1E, S1E). Autofluorescence excited at 355nm and imaged between 400-600nm showed an unusually bright extramitochondrial component in GBA1-PD fibroblasts (Fig 1F) that was significantly greater than control cells. Spectral scanning and linear unmixing separated the expected mitochondrial NADH signal with an emission peak at 450nm and an extensive non-mitochondrial signal with a peak emission at 480nm, attributed to accumulated lipofuscin. Lipofuscins are cytoplasmic granules generated as a consequence of autophagy and phagocytosis processes, which show auto-fluorescence over a broad spectrum ranging from 480nm to 700nm when excited by ultraviolet or blue light[15]. While the accumulation of lipofuscin serves as an indicator of ageing, abnormal accumulation is consistent with impaired lysosomal acidification and defective autophagy[64]. Accumulation of lipofuscin is also a hallmark of Batten Disease (neuronal ceroid-lipofuscinoses), a severe early-onset neurodevelopmental disorder with progressive neurodegeneration also associated with

lysosomal dysfunction [27]. These data collectively indicate significant lysosomal dysfunction in the GBA1-PD cells.

Mitochondria are dysfunctional in cells with GBA1-PD mutations

To determine whether the impaired lysosomal activity in the *GBA1* mutations has a secondary impact on mitochondrial form and function, we measured mitochondrial membrane potential (ΔΨm) using the potentiometric fluorescent reporter tetramethyl-rhodamine methyl ester (TMRM). ΔΨm was significantly reduced in E326K and N370S *GBA1* mutant DA neurons and fibroblasts (Fig 2A, S2A, C). The lower ΔΨm was accompanied by mitochondrial fragmentation in the N370S and E326K DA neurons and fibroblasts (Fig 2Aii c,d, S2Aii b). Ultrastructure analysis using electron microscopy revealed significant differences in mitochondrial morphology in the *GBA1* mutant neurons, including reduced cristae density and increased mitochondrial area, indicating mitochondrial swelling in the *GBA1* mutant iPSC DA neurons (Fig 2B). Measurements of oxygen consumption rates using the 'Seahorse' respirometry system revealed ~40% decrease in basal oxygen consumption rate in the *GBA1* mutant DA neurons with the isogenic controls (Fig 2C). To exclude changes in mitochondrial mass and to explore the substrate dependence of mitochondrial respiration, we used mitochondria isolated from the cultures. This allowed measurements of respiratory rates with different substrates, favouring complex I (pyruvate/malate) or complex II (rotenone/succinate). ADP-stimulated respiration (State 3) rate using both CI and CII-dependent substrates was significantly reduced in the *GBA1* mutant neurons compared to the control neurons (Fig 2D, S2C). Western Blots of the OXPHOS complex proteins using a cocktail of antibodies to respiratory chain proteins, revealed a significant increase in the expression of Complex IV in E326K DA neurons (Fig 2Eii a and S2Dii a) and increased expression of Complex I proteins in N370S neurons compared to the isogenic controls (Fig 2Eii b and S2Dii b). Expression levels of the other respiratory chain proteins were unaltered in the E326K and N370S DA neurons. None of these data suggested any defect in complex I assembly or function. These data collectively point to impaired mitochondrial bioenergetic function in fibroblasts and neurons carrying *GBA1* mutations.

Mitophagy is impaired in cells with GBA1-PD mutations

We then set out to explore the underlying mechanisms that link impaired lysosomal function to impaired mitochondrial bioenergetics in the GBA1-PD fibroblasts and DA neurons. A logical mechanism linking impaired lysosomal function with mitochondrial dysfunction might operate through dysfunctional mitophagy and our earlier work also established dysfunctional mitophagy in *Gba1* KO mice[49]. We quantified mitophagy using the dual excitation probe mt-Keima (Fig 3A). mt-Keima is a pH-sensitive probe that measures the fraction of mitochondria in neutral (pH 7 - 7.8 in the mitochondrial matrix) versus acidic pH (pH 4.5-4.7 in lysosomes) environment[67]. The mt-Keima signal ratio was significantly reduced in fibroblasts and DA neurons in the fibroblasts and DA neurons carrying both the GBA1-N370S and GBA1-E326K mutations indicating impaired mitophagy (Fig 3Aii. S3Aii, Bii). Western blotting to quantify the status of autophagy pathways in the *GBA1* mutant neurons revealed increased LAMP1 levels in E326K and N370S neurons, along with increased MTORC1 phosphorylation in the

two mutant types. While LC3 flux, and expression of p62 and TOM20 were increased in the E326K mutant iPSC DA neurons, these were not significantly altered in the N370S DA neurons (Fig 3B). Since the lysosomal pH is increased in GBA1-PD cells (Fig 1D), the reduced mt-Keima signal in GBA1-PD cells could be attributed either to the altered lysosomal pH or to the impaired fusion of autophagosomes to lysosomes. To address this, we performed triple staining of fibroblasts against citrate synthase (CiS, for mitochondria), LAMP1 (for lysosomes), and LC3 (for autophagosomes). Subsequent imaging revealed that although there was no significant difference in mitophagosome (mitochondria and autophagosome colocalisation) density between *GBA1* mutant and control fibroblasts, mitolysosome (colocalisation of mitochondria and lysosomes) density was significantly increased in the *GBA1* mutant fibroblasts (Fig 3C). Characterisation of electron micrographs for specific autophagic vesicle types based on Neikirk et al.,2023[47], showed that autophagic vesicles, specifically the autolysosome and lysosome number, were significantly increased in both *GBA1* mutant fibroblasts and neurons. (Fig 3Dii, S3Cii a and b). From the micrographs, the autophagosomes also appeared to be fully enclosed, ruling out incomplete phagophore formation as the underlying mechanism of autophagy defect. These data indicated that mitophagy is significantly impaired in cells carrying the GBA1-PD mutations and the decrease in mitophagy is likely due to impaired pH and not improper phagophore formation.

V-ATPase complex formation is impaired in GBA1-PD

Since our data showed an accumulation of lysosomes and autolysosomes in GBA1-PD fibroblasts and iPSC-DA neurons, we suspected this was a result of impaired lysosomal acidification. Assembly of the pH regulatory component in lysosomes – the Vacuolar-type H+ ATPase (V-ATPase) is regulated by MTORC1[53], which was constitutively phosphorylated in the GBA1-PD mutant cells. Ratto et al.[53] demonstrated that under nutrient-rich conditions, MTORC1 is distributed in the cytosol, enabling the peripheral $ATP6V_1$ to bind to the membrane-bound $ATP6V_0$ domain, forming a functional V-ATPase complex allowing proton exchange and acidification of the lysosomes. Upon nutrient deprivation, MTORC1 is phosphorylated and remains on the lysosomal membrane, preventing the formation of a functional V-ATPase complex[53]. While the V-ATPase maintains lysosomal pH, disruption of the complex does not hamper autolysosome formation[43]. Total protein estimation through western blotting revealed no significant difference in the expression of $ATP6V_0D2$ and $ATP6V_1A$ or $ATP6V_1H$ between the control and mutant DA neurons (Fig 4A). To examine their expression levels in lysosomes specifically, we performed a lysosomal enrichment assay and probed for pMTORC1, LAMP1, and the $ATP6V_0$ and $ATP6V_1$ components (Fig 4Bi). pMTORC1 expression was increased up to two-fold, and LAMP1 expression was increased ~1.5 fold in the GBA1-mutant DA neurons. However, $ATP6V_1A$ expression was reduced by ~40% and $ATP6V_1H$ by ~15% within the lysosomes fractionated from *GBA1* mutant DA neurons, while $ATP6V_0D2$ levels remained unchanged between the control and mutant iPSC-DA neurons (Fig 4Bii). Furthermore, overnight treatment of *GBA1* iPSC-DA neurons with the MTORC1 inhibitor rapamycin (200nM) decreased the pMTORC1 and LAMP1 levels, while increasing $ATP6V_1A$ and $ATP6V_1H$ expression in the lysosomes and the $ATP6V_0D2$ levels remained constant (Fig 4Bi b and Bii).

211 In order to assess the V-ATPase assembly, we transfected the cells with ATP6V_1B2-
212 mNeongreen and ATP6V_0a3-mScarlet and quantified their FRET interaction using
213 fluorescence lifetime imaging microscopy (FLIM)[66]. The data were best fit to a
214 biexponential decay function. The ATP6V_0a3 construct utilises the more rapidly maturing but
215 photophysically heterogeneous acceptor variant mScarlet-I[3]. This exhibits at least two
216 fluorescence lifetimes, meaning the biexponential decay of the donor is an oversimplification
217 given the likelihood of contrasting FRET rates to each acceptor species [4, 41]. The results are
218 therefore presented as the mean (amplitude weighted) fluorescence lifetime -τ_m- which will
219 nevertheless respond to variations in FRET without having to interpret the meaning of
220 individual decay components and amplitudes. τ_m of ATP6V_1B2-mNeongreen averaged
221 617.72± 25.3 ps in control fibroblasts but increased to 760.88± 20.36 ps in N370S and 811.03±
222 17.04 ps in E326K mutant fibroblasts, indicating an increased distance between ATP6V1B2-
223 mNeongreen and ATP6V0a3-mScarlet signalled by a reduction in FRET. Overnight treatment
224 with 200nM rapamycin significantly decreased τ_m to 652.7± 19.69 ps and 726.05± 21.2 ps in
225 E326K and N370S fibroblasts respectively while the τ_m control fibroblasts was at 590.5± 32.7
226 ps (Fig 4C). To validate the subcellular localisation process within a condensed timeframe, we
227 administered 1 μM rapamycin to the cells and performed FLIM every 10 minutes for 40
228 minutes. The mean fluorescence lifetime of ATP6V1B2-mNeongreen exhibited a progressive
229 decline in the *GBA1* mutant fibroblasts, decreasing from ~850 ps at 0 min to ~580 ps at 40
230 minutes, while τ_m in control fibroblasts showed only a small reduction, decreasing from ~675
231 ps at 0 min to ~588 ps at 40 minutes (Fig 4Dii). The FLIM-FRET data thus confirmed impaired
232 assembly of the V -ATPase complex in *GBA1* mutant cells.

233 All these data are consistent with a model in which phosphorylation of MTORC1 at the
234 lysosome membrane limits the formation of a functional V-ATPase complex in the GBA1-PD
235 cells. Employing rapamycin as a potent MTORC1 inhibitor reduced MTORC1 activity and
236 facilitated the formation of a functional V-ATPase complex.

237 **Acidification of lysosomes is sufficient to restore lysosomal, mitochondrial function and**
238 **mitophagy in GBA1-PD**

239 Our data show that *GBA1* mutations lead to significantly impaired lysosomal acidification and
240 mitophagy and suggest that this failure of cellular homeostasis may underlie the mitochondrial
241 dysfunction seen in GBA1-PD cells. We therefore wondered whether restoring lysosomal pH
242 could rescue these defects in GBA1-PD cells. Since impaired V-ATPase complex formation
243 may be a consequence of MTORC1 hyperphosphorylation, we explored the impact of treatment
244 with rapamycin (overnight treatment with 200 nM) on lysosomal and mitochondrial function.
245 As an independent pH modulator, we employed novel poly(ethylene tetrafluorosuccinate-co-
246 succinate) nanoparticles (NPs), which acidify lysosomes[73].

247 We first validated the effects of rapamycin and the nanoparticles in patient-derived fibroblasts
248 (Fig S4). To confirm that the NPs were localised to the lysosomes, we loaded the fibroblasts
249 with rhodamine-tagged NPs and stained the cells with Lysotracker blue DND22 (Fig S4A)
250 which confirmed the localisation of the NPs to lysosomes. Overnight treatment with 180 μg/mL
251 acidic NPs composed of poly(ethylene tetrafluorosuccinate-co-succinate) restored lysosomal

pH in *GBA1* mutant cells to levels comparable to those of control fibroblasts as measured using the pH-sensing ratiometric probe Lysosensor Yellow/Blue DND160. Treatment with non-acidic control NPs did not significantly affect the lysosomal pH in the *GBA1* mutant fibroblasts (Fig. S4B, C). TMRM staining demonstrated that both rapamycin and the acidic NPs significantly rescued the ΔΨm in the mutant fibroblasts (Fig S4F, G). We also found that the ΔΨm was increased in control 2 and E326K fibroblasts upon control NP treatment (Fig S4G). We wondered whether the effect of control NPs on ΔΨm could be due to the succinate component in the poly(ethylene succinate) control NPs. However, treatment with 3mM Diethyl Succinate for 30 minutes did not have any effect on the ΔΨm in control and *GBA1* mutant fibroblasts (Fig S4H).

We then assessed the impact of rapamycin and acidic NPs on *GBA1* mutant iPSC-derived DA neurons (Fig 5). Treatment with 200nM rapamycin and 180 µg/mL acidic NPs restored lysosomal pH, ΔΨm, and mitophagy in the E326K and N370S iPSC DA neurons (Fig 5A, B, C). Although there was no change in GBA1 expression levels, GCase activity was increased in *GBA1* mutant DA neurons following treatment with either rapamycin or acidic NPs (Fig S4 D, E). Additionally, western blotting of OXPHOS complexes indicated that the reduced mitochondrial Complex IV levels in E326K DA neurons and the reduced Complex I levels in the N370S DA neurons were normalised upon treatment with either rapamycin or acidic NPs. (Fig S4I).

As rapamycin restores the assembly of the V-ATPase complex in *GBA1* mutant cells (Fig 4D-F), we asked whether the acidic NPs also function through the V-ATPase complex formation. FLIM-FRET experiments conducted on control and acidic NP-treated *GBA1* mutant fibroblasts transduced with ATP6V_1B2-mNeongreen and ATP6V_0a3-mScarlet plasmids demonstrated a further increase in the τ_m of ATP6V1B2 in both control and mutant fibroblasts treated with acidic NPs, confirming that the acidic NPs operate independently of V-ATPase (Fig S4J).

Thus, the data presented here suggest that constitutive phosphorylation of MTORC1 in GBA1-PD cells leads to impaired lysosomal pH and compromised lysosomal proteolytic function. This results in the accumulation of mitolysosomes and impaired mitophagy. The compromised mitophagy culminates in mitochondrial dysfunction in *GBA1* mutant cells. Furthermore, inhibiting MTORC1 activity or pharmacologically increasing lysosomal pH using acidic NPs enhances lysosomal proteolytic activity, rescuing mitochondrial dysfunction in *GBA1* mutant iPSC-DA neurons and fibroblasts.

Discussion:

We report a range of abnormalities in the lysosomes and mitochondria of GBA1-PD fibroblasts and iPSC-DA neurons carrying E326K or N370S *GBA1* mutations. Given that GBA1 is a lysosomal resident enzyme, we hypothesised that mitochondrial dysfunction is likely to reflect a primary lysosomal defect. We used the ratiometric probe Lysosensor Yellow/Blue DND 160 to measure lysosomal pH. When calibrated, these measurements revealed that lysosomal pH in control cells ranged from 4.74 ± 0.03 to 4.77 ± 0.02, while in mutant cells it showed a significant shift to a range of 4.89 ± 0.02 to 5.06 ± 0.03. Reports in the literature indicate that the optimal pH for lysosomal function ranges between 4.2 and 4.8, depending on the cell type

[52, 74]. Although the difference between control and mutant cells seems modest, the data we present suggest that this difference in mutant cells is functionally significant. In line with other studies, we observed a pH-dependent decrease in the lysosomal enzyme activity, an increase in lysosomal number, and disruption of mitophagy and mitochondrial metabolism [2, 7, 24, 31, 40, 46, 51, 58].

Very few reports discuss mitochondrial abnormalities associated with GBA1-PD [1, 24, 25, 32, 54], and even fewer discuss mitophagy [35]. We noted reduced $\Delta\Psi m$ and mitochondrial fragmentation alongside swollen mitochondrial structures, decreased cristae density, and a reduced oxygen consumption rate, all indicating dysfunctional mitochondrial oxidative phosphorylation. This was also associated with reduced mitophagy in the E326K and N370S GBA1-PD fibroblasts and iPSC-DA neurons.

Numerous studies have suggested mechanistic evidence for a connection between PD and *GBA1* mutations. For example, dysfunctional mitochondria in primary neurons and astrocytes were described in the *Gba1* mouse knockout model, associated with an impaired autophagy-lysosomal pathway, resulting in the accumulation of ubiquitinated proteins and α-synuclein[49]. Various studies have explored the mechanisms behind the PD pathology in *GBA1* mutant models. A recent study emphasised that decreased GCase activity in GBA1-PD midbrain dopaminergic neuronal cells leads to defective modulation of the untethering protein TBC1D15, which regulates Rab7 GTP hydrolysis for contact untethering. This impairment results in prolonged mitochondria-lysosome contacts, potentially affecting mitochondrial dynamics and function in GBA1-linked PD[32]. Baden et al. proposed an alternative function of GBA1 in the mitochondria in maintaining the integrity of complex I and support of energy metabolism[1], although in the present study we found no evidence for mitochondrial localisation of GBA1 nor impaired assembly of complex I.

Our respirometry assays using isolated mitochondria revealed a marked reduction in both maximal respiratory capacity and ATPase-linked oxygen consumption in GBA1-E326K and N370S mutant DA neurons, upon stimulation with complex I (pyruvate/malate) and complex II (rotenone/succinate) substrates. The impairment across both complexes points to a global mitochondrial dysfunction, potentially arising from structural abnormalities such as mitochondrial enlargement and decreased cristae density—features observed in these mutants—or as a downstream consequence of lysosomal dysfunction. Notably, lysosome-related mitochondrial impairment has also been reported in Tre-2/Bub2/Cdc16 (TBC1) domain containing Kinase (TBCK) encephaloneuronopathy, supporting a broader link between lysosomal defects and mitochondrial pathology[68].

Recent evidence suggests that the primary cause of the pathologies associated with lysosomes and mitochondria in PD is the *GBA1* mutation. There appears to be a correlation between the onset of PD and lysosomal dysfunction caused by impaired GCase activity. Dysfunctional lysosomes disrupt cellular signalling networks, metabolic processes, autophagy, and the regulation of calcium (Ca^{2+}) signalling, all of which may contribute to PD pathology[17, 31, 34, 46, 59]. Furthermore, both lysosomal function and autophagy are intrinsically dependent on lysosomal acidification, which is influenced by the pH-dependence of lysosomal enzyme activity and substrate degradation, as well as the regulation of lysosomal calcium efflux[63].

335 Li et al. also suggest that autophagy in L444P mutant GBA1-PD neurons is impaired at two
336 stages: the initial autophagy stage and the lysosomal degradation stage. While these reports
337 indicate a relationship between *GBA1* mutations and autophagic, lysosomal, and mitochondrial
338 dysfunction, a mechanistic dissection of these multi-organellar dysfunctions is lacking.

339 Dysregulation of the MTORC1 pathway is reported in various neurodegenerative diseases,
340 including PD and Alzheimer's disease[36, 72]. A recent study by Chen et al. suggests that
341 hyperphosphorylation of MTORC1 in striatal inhibitory neurons diminishes the disruption of
342 dopamine receptor activity, alongside odour preference, in transgenic mice [11]. Liu et al.
343 demonstrate the role of MTORC1 in dopamine dynamics and synaptic plasticity[37]. These
344 results elucidate the additional impacts of increased phosphorylated MTORC1 on PD.
345 Kaempferol, an MTORC1 inhibitor, has also been shown to promote autophagy and to protect
346 DA neurons in the MPTP-induced C57BL/6J–PD mouse model [38]. All this literature suggests
347 that hyperphosphorylated MTORC1 may play a central role in the development of PD
348 associated with *GBA1* mutations. Our study also indicates increased MTORC1 phosphorylation
349 in GBA1-PD fibroblasts and iPSC-DA neurons. While the link between MTORC1
350 hyperphosphorylation and *GBA1* mutations is unclear, it may reflect a cellular stress response
351 to lipid substrate accumulation, indicating nutrient deprivation under *GBA1* mutant
352 conditions[19, 29, 61].

353 Recent evidence underscores the significance of impaired lysosomal acidification in various
354 disease processes. Notably, impaired lysosomal acidification is proposed to be a critical factor
355 in the pathogenesis of multiple neurodegenerative diseases[13, 24, 27, 56]. Mutations in
356 presenilin-1 (*PS1*) associated with familial Alzheimer's disease have been demonstrated to
357 inhibit the lysosomal acidification of human *PS1* mutant fibroblasts, resulting in chronic
358 alterations in autophagy and degradation, which may be restored through lysosomal
359 reacidification[14]. Furthermore, it has been established that individuals with Down Syndrome,
360 who are predisposed to early-onset dementia resembling Alzheimer's disease, exhibit increased
361 levels of the β-cleaved carboxy-terminal fragment of the amyloid precursor protein due to the
362 presence of an additional chromosome 21, which impairs lysosomal acidification and
363 functionality via the inhibition of V-ATPase[30]. Collectively, these studies illuminate the
364 connections between the impairment of lysosomal acidification in autophagic pathways and
365 the pathogenesis of neurodegeneration, thereby presenting potential therapeutic avenues for
366 targeting lysosomal function and pH to mitigate these debilitating diseases. Acidic NPs in the
367 form of poly(lactic-co-glycolic acid) (PLGA) acidic NPs have been previously used to reduce
368 lysosomal pH and disease progression in cells derived from GBA1-N370S PD patient
369 fibroblasts and in PD mouse models[5]. Additionally, poly-succinate acidic NPs used in this
370 study have been employed to restore lysosomal pH and rehabilitate metabolic and lysosomal
371 functions in cases of non-alcoholic fatty liver disease[73].

372 As an MTORC1 inhibitor[56], rapamycin also acts as a prominent inducer of mitophagy and
373 has been demonstrated to mitigate mitochondrial dysfunction in various disease models
374 through inhibition of the MTOR pathway[9, 75]. Consistent with findings from other studies,
375 we found that rapamycin rescues mitophagy and mitochondrial function in GBA1-PD
376 fibroblasts and DA neurons as well. This could either be due to the role of MTOR as a regulator

of mitochondrial function[16, 45] or a downstream effect of lysosomal acidification by MTOR inhibition. To establish whether impaired lysosomal acidification is the cause of these dysfunctions, we employed an independent pH modulator in the form of novel acidic poly-succinate NPs, which rectify lysosomal pH in the cells while enhancing lysosomal and mitochondrial functions in GBA1-PD fibroblasts and DA neurons. Our data confirmed the efficacy of acidic NP treatment on lysosomal pH *in vitro*. We show that the ratio of alkaline vs acidic lysosomes decreased significantly in all mutants and most controls after the acidic NP treatment, demonstrating a decrease in mean lysosomal pH. The effect on controls could be due to the alkalinisation of the lysosomes with age, which can be reversed by the acidic NP treatment in healthy cells[10]. Importantly, treatment with acidic NP successfully eliminated the differences in lysosomal pH between the *GBA1* mutants and the controls. We conclude that the restoration of lysosomal acidification in the mutant cells improved lysosomal function.

Lysosomal acidification also rescued GCase activity in the cells despite mutations in the GBA1 protein. Other studies have also demonstrated the restoration of GCase activity despite *GBA1* mutations under acidic pH conditions[50, 65, 71]. The N370S mutation results in a structurally rigid protein with reduced intralysosomal stability and reduced GCase activity[71]and the E326K mutation has little effect on the active catalytic site of the protein but affects the dimerisation and quaternary structure formation due to folding defects, likely leading to a mild reduction in GCase activity at higher pH levels[50]. GCase activity depends on protonation of amino acids at the active sites and due to interaction of the protein with activators like saposin C[42], which is affected due to the mutation[50, 57]. Restoring the acidic pH in the lysosomes helps restore functional GCase activity despite the mutations possibly by stabilising protein structure, improving folding and optimising the active-site ionisation[48, 50]

To explore whether altered lysosomal pH is related to mitochondrial dysfunction in GBA1-PD, we evaluated ΔΨm, redox levels, and oxidative phosphorylation (OXPHOS) protein levels following treatment with NPs. Our results reveal a significant rescue of ΔΨm among GBA-PD mutants after acidic NP treatment, indicating improved mitochondrial function. When compared to untreated healthy controls, the difference in ΔΨm was no longer statistically significant in the mutants following treatment with acidic NPs. It is noteworthy that some control samples also exhibited alterations due to acidic NP treatment, resulting in a small but significant increase in ΔΨm. We also found a significant increase in ΔΨm in control 2 and E326K fibroblasts upon control NP treatment. Since the NPs are composed of poly(ethylene-succinate), we suspected this could be a substrate-mediated (succinate) effect in control NP treated conditions. However, 30-minute treatment with 3mM Diethyl Succinate did not alter the ΔΨm in the control or mutant fibroblasts. Rescuing lysosomal pH also improved mitophagy in the GBA1-PD fibroblasts and iPSC-DA neurons.

Conclusions:

We have explored the relationship between lysosome biology, pH, mitophagy and mitochondria in cells carrying PD-associated mutations of *GBA1*. A detailed examination of the pathophysiology of these cells reveals a range of abnormalities in the lysosomes, including reduced GCase activity, an increased lysosomal number, impaired lysosomal acidification, and

418 impaired pH-dependent lysosomal proteolytic activity. Mitochondrial dysfunction is reflected
419 by reduced mitochondrial membrane potential, swollen, fragmented mitochondria, decreased
420 cristae density, and the accumulation of abnormal mitochondria, along with a reduced oxygen
421 consumption rate. We also found a decrease in mitophagy and an accumulation of
422 autolysosomes in the GBA1-PD cells. We show that increased pMTORC1 on the lysosomal
423 membrane, possibly due to accumulation of substrates in the lysosomes, causing nutrient
424 deprivation, hinders the formation of a functional V-ATPase complex in GBA1-PD cells,
425 thereby compromising lysosomal acidification. We found that inhibiting MTORC1 using
426 rapamycin rescues functional V-ATPase formation and lysosomal pH in the GBA1-PD neurons
427 and rescues mitophagy and mitochondrial function. Independent modulation of lysosomal pH
428 using acidic poly-succinate NPs, restored lysosomal pH, rescued mitophagy and restored
429 mitochondrial function in the GBA1-PD fibroblasts and iPSC-DA neurons (Fig 6). Since
430 rapamycin has broad effects, the comparison to NPs is valuable, adding a translational value
431 for future applications. We thus unravel the mechanism behind impaired lysosomal pH in
432 GBA1-PD cells and demonstrate that restoring lysosomal pH is sufficient to rescue both
433 lysosomal and mitochondrial dysfunction, along with mitophagy in GBA1-PD fibroblasts and
434 iPSC-DA neurons.

435

436 **Figure legends:**

437 **Figure 1: Lysosomal abnormalities in GBA1-PD DA cells-** Representative western blot
438 images of GBA1 protein expression (Ai) and quantification (Aii a,b) in isogenic control and
439 GBA1-E326K and N370S DA neurons. GCase activity in GBA1-E326K (Bi a) and GBA1-
440 N370S (Bi b) DA neurons and respective isogenic controls. Representative ratioed images (Ci
441 a, b) and quantification of fluorescence ratio of GBA1-E326K (Cii a) and GBA1-N370S (Cii
442 b) DA neurons and respective isogenic controls labelled with Lysosensor Yellow/Blue DND
443 160 indicating lysosomal pH in cells. D) Histogram depicting mean lysosomal pH values in
444 *GBA1* mutant fibroblasts. Representative confocal images (Ei a,b) and quantification of relative
445 intensity of GBA1-E326K (Eii a) and GBA1-N370S (Eii b) DA neurons and respective
446 isogenic controls stained with DQ-Red BSA indicative of proteolytic activity. Representative
447 confocal images (Fi) and quantification (Fii) of lipofuscins which are seen upon
448 autofluorescence. Data represented as mean±SEM; n=3; Statistics:**** - $p<0.001$; *** -
449 $p<0.005$; ** - $p<0.01$, * - $p<0.05$; ns – not significant; Mann-Whitney's T test, One-way
450 ANOVA.

451 **Figure 2: Mitochondrial dysfunction in GBA1-PD DA neurons:** Representative confocal
452 images of GBA1-E326K (Ai a) and GBA1-N370S (Ai b) DA neurons along with isogenic
453 controls stained with TMRM and subsequent quantification of fluorescent intensity to measure
454 $\Delta\Psi m$ (Aii a, b) and mitochondrial fragmentation count (Aii c,d). Representative
455 ultramicroscopic images of isogenic control and GBA1-E326K (Bi a) and GBA1-N370S (Bi
456 b) DA neurons and subsequent quantification of morphological parameters including average
457 number of mitochondria, average mitochondrial area and average cristae density in
458 mitochondria (Bii a-f). The white arrow indicates normal mitochondria; black arrow indicates
459 abnormal mitochondria. Histograms representing the basal respiration rate in *GBA1* mutant
460 iPSC-DA neurons from GBA1-E326K (C a) and GBA1-N370S mutant lines(C b) and
461 respective isogenic controls. Representative seahorse plots showing oxygen consumption rates
462 in iPSC-DA neurons from GBA1-E326K (Di a) and GBA1-N370S (Di b) DA neurons and
463 respective isogenic controls, using various substrates. Histograms representing State 3(ATP
464 Production) in mitochondria isolated from GBA1-E326K (Dii a) and GBA1-N370S (Dii b) DA
465 neurons and isogenic controls, as measured by seahorse assay. E i and ii) Representative
466 immunoblotting images (Ei) with subsequent quantification of OXPHOS complex proteins in
467 GBA1 E326K (Eii a) and N370S (Eii b) DA neurons. Data represented as mean±SEM; n=3;
468 Statistics:**** - $p<0.001$; *** - $p<0.005$; ** - $p<0.01$, * - $p<0.05$; ns – not significant; Mann-
469 Whitney's T-test, One-Way ANOVA or Two-Way ANOVA.

470 **Figure 3: Mitophagy defects in GBA1-PD DA neurons:** Representative images of GBA1-
471 E326K (Ai a)and GBA1-N370S (Ai b) DA neurons and isogenic controls transduced with mt-
472 Keima plasmid and imaged with excitation at 458 and 543nm and subsequent quantification of
473 the ratio of signals at 543/458nm (Aii a,b). Representative western blot images of *GBA1*
474 mutant and isogenic control lysates probed for autophagic proteins (Bi) and subsequent
475 quantification of protein levels (Bii a,b) Representative Immunofluorescence images of
476 Control and N370S fibroblasts probed against Citrate Synthase (CiS), LAMP1 and LC3,
477 labelling mitochondria, lysosomes and autophagosomes respectively (Ci) and subsequent

478 quantification of colocalisation co-efficient of mitophagosomes (Cii a) and mitolysosomes(Cii
479 b). Representative TEM images (Di) and quantification (Dii) of control and E326K mutant
480 fibroblasts capture different autophagy phases in the cells. Black arrows indicate lipofuscins,
481 yellow arrows indicate autolysosomes, red arrows indicate autophagosomes, and green arrows
482 indicate lysosomes in the cells. Data represented as mean±SEM; n=3; Statistics:**** -
483 p<0.001; *** - p<0.005; ** - p<0.01, * - p<0.05; ns – not significant; Mann-Whitney's T-test,
484 One-Way ANOVA.

485 **Figure 4: Impaired V-ATPase complex formation in GBA1-PD cells-** Representative
486 images of western blots (Ai) and quantification of protein levels in total cell lysates from
487 isogenic control and GBA1-E326K (Aii a) and GBA1-N370S (Aii b) mutant DA neurons
488 probed against LAMP1 and V-ATPase complex proteins. Representative immunoblotting
489 images of cell supernatant and lysosomes separated by lysosome enrichment assay in untreated
490 (Bi a) and 200nM rapamycin-treated (Bi b) GBA1-PD DA neurons and isogenic controls, and
491 subsequent quantification (Bii) of V-ATPase complex proteins, pMTOR. Representative FLIM
492 images of ATP6V_1B2-mNeonGreen in control and GBA1-PD fibroblasts co-transfected with
493 ATP6V_0a3-mScarlet and treated with/without 200nM rapamycin (Ci) and subsequent
494 quantification of mean lifetime (τ_m) (Cii b). Cii a) Representative decay plots and exponential
495 fit of ATP6V1B2-mNeongreen in the Control and N370S and E326K mutant fibroblasts. D i)
496 Time point images of ATP6V_1B2-mNeongreen in control and GBA1-PD fibroblasts co-
497 transfected with ATP6V_0a3-mScarlet and treated with 1 μM rapamycin and imaged over a
498 period of 40 mins and subsequent quantification of τ_m shown in Dii) Data represented as
499 mean±SEM; n=3; Statistics:**** - p<0.001; *** - p<0.005; ** - p<0.01, * - p<0.05; ns – not
500 significant; Mann-Whitney's T-test, One-Way ANOVA or Two-Way ANOVA.

501 **Figure 5: Rapamycin and acidic NPs rescue lysosomal and mitochondrial dysfunction in**
502 ***GBA1* mutant DA neurons:** Representative ratioed images of GBA1-E326K (Ai a) and
503 GBA1-N370S (Ai b) DA neurons and respective isogenic controls treated overnight with
504 200nM rapamycin or 180μg/mL acidic NPs and stained with Lysosensor Yellow/Blue DND
505 160 (Ai a,b) and quantification of fluorescence ratio (Aii a-d) indicating lysosomal pH.
506 Representative confocal images of GBA1-E326K (Bi a) and GBA1-N370S (Bi b) DA neurons
507 and respective isogenic controls treated with 200nM rapamycin or 180μg/mL acidic NPs and
508 stained with TMRM to measure changes in ΔΨm (Bii a-d). Representative confocal Images of
509 GBA1-E326K (Ci a) and GBA1-N370S (Ci b) DA neurons and respective isogenic controls
510 treated with 200nM rapamycin or 180μg/mL acidic NPs and probed with mt-Keima plasmid
511 and imaged with excitation at 458 and 543nm and subsequent quantification of the ratio of
512 signals at 543/458nm (Cii a-d). Data represented as mean±SEM; n=3; Statistics:**** -
513 p<0.001; *** - p<0.005; ** - p<0.01, * - p<0.05; ns – not significant; One-Way ANOVA.

514 **Figure 6: Cartoon to illustrate the proposed pathophysiological cascade in GBA1-related**
515 **Parkinson's Disease and how the phenotype can be corrected by targeting lysosomal pH**
516 **-** GBA1-PD cells exhibit a range of abnormalities in lysosomal biology, including reduced
517 GCase activity, increased lysosomal numbers, elevated lysosomal pH, and decreased pH-
518 dependent proteolytic activity. Mitochondrial dysfunction is evidenced by a decreased ΔΨm,
519 decreased oxygen consumption rate, swollen mitochondria, reduced cristae density, and the

accumulation of abnormal mitochondria. Mitophagy is suppressed and autolysosomes accumulate within the GBA1-PD cells. Restored acidification of lysosomes with rapamycin or acidic poly-succinate NPs enhances lysosomal function and improves mitophagy, thereby rescuing mitochondrial dysfunction in GBA1-PD fibroblasts and lysosomes.

Supplementary Figure 1: Lysosomal abnormalities in GBA1-PD DA neurons and fibroblasts- GBA1 protein expression (Ai) and subsequent quantification of GBA1 levels in control and GBA1-E326K (Aii a) and N370S (Aii b) DA neurons. GCase activity in GBA1-E326K (Bi a) and GBA1-N370S (Bi b) DA neurons and fibroblasts (Bii). Representative ratioed images of GBA1-E326K and GBA1-N370S fibroblasts (Ci) and DA neurons (Di a,b) stained with Lysosensor Yellow/Blue DND 160, subsequent quantification of fluorescence ratio measuring lysosomal pH (Cii, D ii a,b). Histogram representing quantification of DQ-Red BSA intensity in GBA1-E326K (E a) and GBA1-N370S (E b) and control DA neurons indicating lysosomal proteolytic activity. Data represented as mean±SEM; n=4; Statistics:**** - $p<0.001$; *** - $p<0.005$; ** - $p<0.01$, * - $p<0.05$; ns – not significant; Mann-Whitney's T test, One-way ANOVA.

Supplementary Figure 2: Mitochondrial dysfunction in GBA1-PD DA neurons and fibroblasts: Representative images of GBA1-E326K and GBA1-N370S fibroblasts (Ai) and DA neurons (Bi a,b) along with controls, stained with TMRM to measure changes in $\Delta\Psi m$ (Aii a, Bii a,b) and the mitochondrial fragmentation count (Aii b). Histograms representing State 3 (ATP Production) in mitochondria isolated from GBA1-E326K (C a) and GBA1-N370S (C b) DA neurons and controls, as measured by Seahorse assay. Representative images of western blots probed for OXPHOS complex proteins (Di) and subsequent quantification of protein expression levels in GBA1 E326K (Dii a) and N370S(Dii b) DA neurons. Data represented as mean±SEM; n=5; Statistics:**** - $p<0.001$; *** - $p<0.005$; ** - $p<0.01$, * - $p<0.05$; ns – not significant; Mann-Whitney's T-test, One-Way ANOVA or Two-Way ANOVA.

Supplementary Figure 3: Mitophagy defects in GBA1-PD DA neurons and fibroblasts: Representative ratioed images of control and GBA1-E326K and GBA1-N370S fibroblasts (Ai) and DA neurons (Bi a,b) transduced with mt-Keima plasmid and imaged imaged with excitation at 458 and 543nm and subsequent quantification of the ratio ratio of signals at 543/458nm respectively (Aii, Bii a,b). Representative TEM images of GBA1-E326K (Ci a) and GBA1-N370S (Ci b) DA neurons and respective isogenic controls depicting autophagic vesicles and subsequent quantification (Cii a,b). Yellow Arrows indicate autolysosomes, red arrows indicate autophagosomes, and green arrows indicate lysosomes in the cells. Data represented as mean±SEM; n=3; Statistics:**** - $p<0.001$; *** - $p<0.005$; ** - $p<0.01$, * - $p<0.05$; ns – not significant; Mann-Whitney's T-test, One-Way ANOVA.

Supplementary Figure 4: Effect of acidic NPs and rapamycin on GBA1 – PD fibroblasts and DA neurons: Representative Confocal images (Ai) of control and mutant fibroblasts treated with Rhodamine-tagged acidic NPs (Rhod-acidic NPs) and stained with Lysotracker Blue and subsequent quantification of colocalisation coefficient (Aii). Representative images of control and GBA1-E326K and GBA1-N370S fibroblasts treated with control and acidic NPs (Bi) and stained with the ratiometric Lysosensor Yellow/Blue DND160 subsequent quantification of fluorescence ratio (Bi) to measure lysosomal pH and. C) Calibration of

lysosomal pH in *GBA1* mutant fibroblasts treated with and without acidic nanoparticles. Representative images of western blots and quantification of GBA1 protein levels in GBA1-E326K (Di a; Dii a,b) and GBA1-N370S (Di b; Dii c,d) DA neurons and respective isogenic controls treated with acidic NPs or rapamycin and probed for GBA1 and B-ACTIN. GCase activity in GBA1-E326K and GBA1-N370S DA neurons and respective isogenic controls treated with Acidic NPs (E a, c)/rapamycin (E b, d). Images representing rapamycin treated (Fi) and Acidic NPs treated (Gi) control and GBA1-E326K and GBA1-N370S fibroblasts and stained with TMRM and subsequent quantification of $\Delta\Psi m$ (Fii and Gii respectively). Histogram representing quantification of mitochondrial membrane potential in *GBA1* mutant and control fibroblasts upon 3mM Diethyl succinate treatment for 30 minutes (H). Representative images of western blots (Ii a,b) and subsequent quantification of OXPHOS complex proteins in GBA1 E326K and N370S DA neurons and respective isogenic controls treated with Acidic NPs (Iii a,b) and rapamycin (Iii c,d). Representative FLIM images of $ATP6V_1B2$-mNeongreen in Control and GBA1-PD fibroblasts co-transfected with $ATP6V_0a3$-mScarlet and treated with/without acidic NPs (Ji) and subsequent quantification of mean lifetime (τ_m) of $ATP6V_1B2$ (Jii). Data represented as mean±SEM; n=3; Statistics:**** - $p<0.001$; *** - $p<0.005$; ** - $p<0.01$, * - $p<0.05$; ns – not significant; Mann-Whitney's T test, One Way ANOVA.

580 **Methodology:**

581 **Cell lines and ethics committee approval:**
582 The human iPSC (hiPSC) and fibroblast lines used in the study, along with their sources, are
583 detailed in Table 1. Fibroblasts were cultured in DMEM (1x) + GlutaMAX™ basal media
584 (Gibco 2206106), 10% (v/v) Foetal Bovine Serum (Gibco 10270098), and 1% antibiotic-
585 antimycotic (Gibco 15240096), and incubated at 37 ºC with 5% CO_2. The media was changed
586 every 72 hours, and the cells were passaged upon reaching 80% confluency using 0.25%
587 Trypsin-EDTA (Gibco 25200056). Passages between 9 and 15 were used for experimental
588 purposes. Human GBA1 patient-derived iPSC lines were cultured under feeder-free conditions
589 on Geltrex-coated 6-well plates, using mTeSR Plus medium and were passaged every 4-5 days
590 with a 0.5 mM EDTA solution or upon reaching 80% confluency. Passage numbers between
591 20 and 30 were employed for differentiation purposes

592 **Human pluripotent stem cell-derived DA neurons**
593 DA neurons were generated from iPSCs using a step-by-step differentiation protocol, as
594 previously described[69]. Briefly, 90-95% confluent hiPSCs were cultured on Geltrex-coated
595 plates and maintained in N2B27 medium, which is a 1:1 mix of Neurobasal (Gibco, 21103049)
596 supplemented with 1X B27 (Gibco, 17504044), Glutamax (Gibco, 35050-038), and 0.5X Anti-
597 anti (Gibco, 15240096), and DMEM-F12 (Gibco, 10565018) supplemented with 1X N2
598 supplement (Gibco, 17502048), 1X MEM Non-Essential Amino Acids (Gibco, 11140-050),
599 0.5X Anti-anti (Gibco, 15420096), 50 µM β-mercaptoethanol (Gibco, 21985-023), and human
600 Insulin Solution (Sigma, I9278). Daily media changes were conducted for the first 14 days. On
601 day 0, the media was supplemented with 5 µM SB431542 (Tocris Bioscience, 1614/10), 2 µM
602 Dorsomorphin (Tocris Bioscience, 3093/10), and 1 µM CHIR99021 until day 2. From day 2 to
603 day 7, 1 µM Purmorphamine (Merck Millipore, SML0868) was added to the mix. From day 8
604 to day 14, CHIR99021 and SB431542 were removed from the medium, and the cells were
605 maintained with Dorsomorphin and Purmorphamine in N2B27. Cells were dissociated with 1
606 mg/mL Dispase (Gibco, 17105041) on days 4 and 14. After patterning for 14 days, the midbrain
607 DA neuronal precursor cells (NPCs) were maintained in N2B27 medium until day 18. On day
608 19, the cells were dissociated with Accutase (Gibco, A1110501) and plated onto Geltrex-coated
609 plates at a density of 2 × 10^5 cells/cm² and terminally differentiated with N2B27 medium
610 supplemented with Compound E (Enzo Lifesciences, ALX-270-415-C250) and 10 µM Rho-
611 kinase inhibitor, Y-27632 dihydrochloride (Tocris, 1254) from day 20 until day 70-75, with
612 media changes twice a week. DA neurons between days 70 and 75 were used for downstream
613 experiments.

614 **Nanoparticle, rapamycin and diethyl succinate treatment**
615 Control and acidic NPs, composed of poly(ethylene-succinate) and poly(ethylene
616 tetrafluorosuccinate-co-succinate) respectively, were obtained from Prof. Mark Grinstaff and
617 Prof. Orian Shirihai. The synthesis of the nanoparticles is described in [73]. The nanoparticles
618 were stored at -80°C in aliquots and thawed fresh prior to treatment. Aliquots of 75 mg/mL
619 nanoparticles were thawed to room temperature, vortexed thoroughly, and added to the cells at
620 a concentration of 180 µg/mL in fresh culture medium for 12-16 hours before the experiment.

621 A stock solution of 200 µM rapamycin (Sigma, R0395) was prepared in DMSO and sterile
622 filtered before being stored as aliquots at -20ºC. This stock solution was diluted to 200 nM in
623 medium before being added to the cells. The cells were treated with 200 nM rapamycin for 12-
624 16 hours before proceeding with the experiments unless mentioned otherwise. Diethyl
625 Succinate (Merck, 112402) was diluted to 3 mM in culture media and sterile-filtered and added
626 onto cells 30 minutes prior to measuring the ΔΨm using TMRM.

627 **Generation of lentivirus and transduction:**
628 pLV-Ef1a-3xHA-ATP6V1B2-mNeonGreen and pLV-Ef1a-3xFlag-ATP6Voa3-mScarlet
629 plasmids were kindly provided by Dr. Wilhelm Palm (EPR 462 and EPR 475, European
630 Plasmid Repository). pHAGE-mt-mKeima was a generous gift from Prof. Richard Youle
631 (131626, Addgene). Lentiviral plasmids were packaged using psPAX2 and pMD2.G in
632 HEK293T cells with Xtremegene-HP transfection reagent (Merck, 6366236001), according
633 to the manufacturer's instructions. The media supernatant containing viruses was collected 48
634 and 72 hours post-transfection and concentrated using Lenti-X transfection reagent (Takara,
635 631231) with overnight incubation, followed by centrifugation at 2000 rpm for 1 hour at 4ºC.
636 The pellet was then resuspended in DMEM-F12 medium and stored at -80ºC for further use.
637 72-96 hours prior to imaging, fibroblasts or DA neurons were treated with lentiviral particles.
638 24 hours post-treatment, the media was replaced with regular culture medium and incubated
639 for another 48 hours before imaging.

640 **Confocal imaging**

641 DMEM-F12 medium (Gibco, 21041025) or BrainPhys medium (Stem Cell Technologies,
642 05796) served as a recording buffer for live cell imaging of fibroblasts and DA neurons. All
643 images were acquired using a Carl Zeiss LSM 880 Confocal Laser Scanning microscope with
644 Zen Black Software and a 63×/1.40 oil immersion lens at 37°C. Fixed and stained fibroblasts
645 were also imaged with the same equipment.

646 **Lysosensor Yellow/Blue DND 160**
647 The cells were washed with DPBS and incubated for 4 minutes in the recording buffer
648 containing 3 µM Lysosensor Yellow/Blue DND 160 (Invitrogen, L7545) at 37°C. After
649 incubation, the dye was washed twice with PBS and imaged in fresh recording buffer using
650 the UV laser at 355 nm. The dual emission maxima of the dye (440 nm/540 nm) were detected
651 using spectral scanning (lambda scan mode) on the Zeiss LSM 880. Images were subsequently
652 linearly unmixed employing the ZEN Black software to separate the 440 nm and 540 nm
653 emission images. The ratio of 440/540 nm was then calculated using the Ratio Plus plugin on
654 ImageJ/Fiji software to determine the lysosomal acidity of fibroblasts and DA neurons

655 **Lysosomal pH measurement**
656 The lysosomal pH was measured using Lysosensor Yellow/Blue DND-160 (L7545, Invitrogen).
657 Fibroblasts cultured on fluorodishes were treated with pH calibration buffer containing
658 Monensin (Sigma, M5273) and Nigericin (Sigma, N7143), with a pH ranging from 3.5 to 7.0
659 and stained with Lysosensor Yellow/Blue DND 160. The cells were incubated with 2 µM for 5
660 minutes at room temperature (RT) and imaged as previously mentioned. The 440/540

661 fluorescence ratio was measured for each calibration buffer. A lysosomal pH calibration curve
662 was established by correlating the 440/540 nm ratio with the corresponding pH values using
663 ImageJ/Fiji software.

664 **Measurement of lysosomal proteolytic activity by DQ Red BSA**

665 The DQ-Red BSA trafficking assay dye (Invitrogen, D12051) was utilised to examine
666 lysosomal proteolytic activity. DA neurones were washed with DPBS, and pre-warmed medium
667 containing DQ-Red BSA was added to the fluorodishes. The dishes were incubated at 37°C for
668 three hours. Following the incubation period, the cells were washed with DPBS and replaced
669 with the recording buffer prior to imaging. Cells stained with DQ-Red BSA were excited using
670 a 561 nm Argon laser, and the emitted fluorescence was collected within the 564–740 nm range.
671 The fluorescence intensity was quantified per cell using ImageJ/Fiji software with consistent
672 threshold settings across all samples.

673 **Measurement of ΔΨm using TMRM**

674 Fibroblast or DA neurons were washed with DPBS and incubated in recording buffer containing
675 20 nM TMRM (Thermofisher Scientific, T668) at 37°C for 30 minutes. Following incubation,
676 fresh recording buffer containing 20 nM TMRM was added before proceeding with imaging.
677 The cells were excited for TMRM fluorescence at 561nm, and images were acquired as Z-
678 stacks. Maximum intensity projection images were then utilised to quantify the fluorescence
679 intensity using ImageJ/Fiji software with consistent threshold settings across all samples. The
680 TMRM images were also used to analyse the mitochondrial morphology [44].

681 **Measurement of Lipofuscin levels**

682 Lipofuscins are excited at 355 nm and fluoresce across a range from 480 to 700 nm[15].
683 Fibroblasts were washed with the recording buffer and imaged using UV illumination at 355
684 nm, with images obtained through spectral scanning. The images were subsequently linearly
685 unmixed using ZEN Black software to separate the 460 nm and 480 nm emission images, thus
686 distinguishing NAD(P)H from lipofuscins. The spectrally unmixed images at 480 nm were then
687 utilised to calculate lipofuscin density per cell using ImageJ/Fiji software.

688 **Colocalization of the Rhodamine-B labelled aNPs with the lysosomes**

689 Rhodamine B-labelled acidic nanoparticles were treated for 12-16 hours prior to imaging the
690 fibroblasts. On the imaging day, cells were washed with the recording buffer and incubated
691 with 50 nM LysoTracker Blue DND-22 dye (Invitrogen, L7525) for 2 hours at 37°C.
692 Following the incubation, the cells were washed with the recording buffer and imaged in fresh
693 buffer. Images were acquired using sequential excitation (405 nm for LysoTracker Blue and
694 561 nm for Rhodamine) and emission ranges set to 420–480 nm and 570–620 nm,
695 respectively. Colocalisation Pearson's coefficient was quantified using ImageJ/Fiji software
696 with consistent threshold settings across all samples.

697 **Measurement of mitophagy using mt-Keima reporter**

698 Measurement of mitophagy was performed as previously described[13]. Untreated fibroblasts
699 and DA neurons were tranduced with lentiviral mt-Keima particles 72 hrs prior to imaging.

700 12-16 hours before imaging, the cells were treated with acidic nanoparticles or rapamycin.
701 The cells were imaged using two sequential excitation wavelengths (458 nm for green
702 fluorescence and 561 nm for red fluorescence) with an emission range of 570–695 nm. The
703 laser power was set at the minimum output to allow the clear visualization of the mt-Keima
704 signal. The ratio of the high F_{543}:F_{458} ratio values were generated using the Ratio Plus plugin
705 in ImageJ/Fiji and was used as an index of mitophagy.

706 **Fluorescence lifetime imaging microscopy (FLIM) quantification of ATP6V$_1$B2-**
707 **mNeonGreen**

708 Fluorescence lifetime imaging was conducted using single-photon excitation on a multimodal
709 time-resolved fluorescence microscope as previously described[22]. This setup encompassed
710 an 80 MHz, near-infrared, femtosecond excitation source (Insight X3, Spectra Physics, Crewe,
711 UK), a second harmonic generation unit (Harmonixx SHG, APE, Berlin, Germany), a laser
712 scanning unit (DCS-120, Becker & Hickl, Berlin, Germany), an inverted microscope (Axio
713 Observer 7, Zeiss, Cambridge, UK) featuring a high numerical aperture objective (Plan-
714 Apochromat 63x/1.4 Oil M27, Zeiss, Cambridge, UK), an ultrafast hybrid detector (HPM-100-
715 07, Becker & Hickl, Berlin, Germany), and time-correlated single photon counting (TCSPC)
716 electronics (SPC-180NX, Becker & Hickl, Berlin, Germany). Images were acquired using 473
717 nm excitation to minimise the ratio of acceptor to donor excitation, along with 500–540 nm
718 emission filtering to isolate fluorescence from the mNeonGreen donor. Photon counts were
719 acquired for two minutes and histogrammed at 14.6ps intervals. Curve fitting analysis was
720 performed in SPCImage (Becker & Hickl, Berlin, Germany).

721 **Lysosomal enrichment assay**

722 A lysosomal enrichment assay was conducted using the Lysosome Enrichment Kit for Tissues
723 and Cultured Cells (Thermo Scientific, 89839) according to the manufacturer's instructions.
724 Briefly, the DA neurons were pelleted and lysed with lysosome enrichment reagent A, which
725 contained 1X protease and phosphatase inhibitors. The solution was then sonicated on ice,
726 applying 12 bursts at 9W of power (Thermo Scientific) and mixed with lysosome enrichment
727 reagent B. The solution was subsequently centrifuged at 500g for 10 minutes. 200 µL of
728 supernatant was then aliquoted for use as cell supernatant for western blotting. Lysosomes were
729 isolated from the remaining solution through gradient centrifugation. The protein
730 concentrations of the lysosomes and cell supernatant were then quantified using a BCA assay
731 and proceeded for western blotting as discussed below.

732 **SDS-PAGE and immunoblotting**

733 Fibroblasts and DA neurons were washed with ice-cold PBS, followed by the addition of 150
734 µl of ice-cold RIPA lysis buffer (Sigma-Aldrich, R0278), which was supplemented with
735 protease inhibitors (Roche 4693116001), PMSF (Sigma, 93482), and phosphatase inhibitors
736 (Roche 4906837001). Cells were scraped using a plastic scraper, and the lysates were
737 transferred to 1.5 ml tubes. The lysates were rotated at 4°C for 30 minutes and sonicated (3
738 cycles, 3 seconds each at 40% amplitude, with 5-minute intervals). Samples were centrifuged
739 at 16,000 g for 30 minutes at 4°C, and the supernatant was collected. Protein concentration
740 was determined using a BCA assay kit (Thermo Scientific, 23227). A total of 20-30 µg of

741 protein was diluted with RIPA buffer and mixed with NuPAGE 4X sample buffer
742 (Invitrogen, NP0007). The samples were heated at 95°C for 5 minutes (for OXPHOS
743 proteins, the lysates were heated at 45ºC for 5 minutes). Proteins were separated on 4–12%
744 NuPAGE Bis-Tris polyacrylamide gels (Invitrogen, NP0335) immersed in MOPS running
745 buffer (Invitrogen, NP0001). Proteins were transferred to PVDF membranes (Millipore,
746 IPFL00010) activated in methanol using a wet transfer system. Membranes were blocked in
747 Superblock blocking buffer (Invitrogen, 37545) for 1 hour at room temperature. Primary
748 antibodies were diluted in 1X blocking buffer and incubated with the membranes overnight at
749 4°C. After three 10-minute washes in TBST, the membranes were incubated with secondary
750 antibodies (Li-COR Biosciences; 1:10000; IRDye® 680RD Goat anti-Mouse IgG, 926-
751 68070; IRDye® 800CW Goat anti-Rabbit IgG, 926-32211) diluted in 1% BSA/TBST for 1
752 hour at room temperature. The membranes were washed three additional times with TBST.
753 Fluorescent signals were developed using a LiCOR Odyssey CLx system. The details of the
754 antibodies are listed in Table 2.

755 **Immunostaining**

756 Fibroblasts were grown on coverslips, treated, and fixed with 4% (w/v) paraformaldehyde.
757 After fixation, the cells were permeabilised with 50 µg/ml digitonin in PBS for 10 minutes.
758 The cells were then washed, blocked with 3% BSA, and incubated with the following primary
759 antibodies: citrate synthase, LAMP1, and LC3 in 3% BSA for 1 hour at room temperature,
760 followed by incubation with Alexa Fluor 488/594/647-conjugated secondary antibodies for 1
761 hour at room temperature. Coverslips were mounted on glass slides, and images were acquired
762 using appropriate excitation and emission filters to capture fluorescent signals. Colocalisation
763 Pearson's coefficient (Mito vs LC3 and Mito vs LAMP1), lysosomal number (LAMP1
764 particles/cell), and autophagosome number (LC3 particles/cell) were quantified using
765 ImageJ/Fiji with consistent threshold settings across all samples. The catalogue number and
766 dilution range of the antibodies are listed in Table 2.

767 **Mitochondrial isolation**

768 Mitochondria were isolated according to the method described earlier [62] and modified for the
769 neuronal cultures. Briefly, DA neuron cell pellets were resuspended in mitochondria isolation
770 buffer (MIB1: 225 mM Mannitol, 75 mM Sucrose, 5 mM HEPES, 1 mM EGTA and 1 mg/ml
771 fatty acid free BSA) and homogenised using a ice-cold Dounce tissue grinder tube (appropriate
772 for 1-1.5 ml homogenisation volume). The homogenate was centrifuged, and the mitochondrial
773 pellet was washed and pellet down in MIB without BSA (MIB2) according to the protocol. The
774 final pellet was resuspended in a very small volume of MIB2, and the protein concentration
775 was determined using BCA Protein assay kit (Thermofisher Scientific, 23227) according to the
776 manufacturer's specifications.The isolated mitochondria were then used for respiratory
777 measurements.

778 **Measurement of oxygen consumption rate**

779 Measurements of mitochondrial respiration were conducted with the Seahorse Bioscience
780 XFe96 bioanalyzer using the Seahorse XF Cell Mito Stress Test Kit (Agilent #103015-100).
781 Final maturation of iPSCs into DA neurons were performed in XF96 cell culture microplates
782 (Agilent #102416-100). On the day of the experiment, the culture medium was replaced with

783 Seahorse XF Base medium (Agilent #103334-100) supplemented with 1 mM pyruvate (Gibco
784 #11360070), 2 mM glutamine (Gibco #25030081) and 10 mM glucose (Gibco #A2494001) and
785 incubated for 30 min at 37 °C in a CO_2-free incubator before loading into the Seahorse Analyser.
786 After measuring basal respiration, the drugs oligomycin (5 μM), FCCP (1.5 μM), and
787 rotenone/antimycin A (0.5 μM/0.5 μM) were added to each well in sequential order. After the
788 assay, cells were stained with Hoechst 33342 (5 μM; Thermo Scientific #62249) for 30 min.
789 ImageXpress was then used to count the number of cell nuclei (cell numbers) in each well and
790 normalised to get the basal respiration rate values.
791 The respiratory measurements of isolated mitochondria from mixed neuronal cultures were
792 performed using a modified method described earlier[6] for Seahorse XFe96 cell culture plates
793 assay. Briefly, 5 or 10 μg of mitochondrial protein was resuspended in 30 μL (1 well) of
794 individual substrate mix (for example, pyruvate/malate substrate + mitochondria assay solution
795 - MAS) and plated into each well. The cell culture plate was centrifuged at 2,000g for 20
796 minutes at 4 °C to form a uniform layer of mitochondria at the bottom. After centrifugation,
797 150 μL of substrate solution was carefully added to each well. Fresh injection solutions were
798 made in MAS without BSA and loaded into the cartridge, and calibrated according to the
799 manufacturer's specifications. After calibration, the culture plate with mitochondria was
800 inserted, and the assay was run essentially as described in the method.

801 **Transmission electron microscopy (TEM)**

802 TEM was performed as previously described [13]. Briefly, fibroblasts and DA neurons grown
803 on coverslips were fixed in electron microscopy (EM) fixative containing 2% glutaraldehyde
804 (EMS, 16365) and 2% paraformaldehyde (EMS, 15710) in 0.1 M sodium cacodylate for 1
805 hour. Following fixation, cells were washed with 0.1 M cacodylate buffer (EMS, 11650) and
806 then fixed in a solution of 1% osmium tetroxide (EMS, 19150) and 1% potassium ferricyanide
807 (EMS, 25120-20) in 0.1 M sodium cacodylate. This was followed by sequential dehydration
808 using ethanol. Coverslips were then embedded in epoxy resin (Araldite Kit, Agar Scientific
809 Ltd., CY212) according to standard protocols. The embedded samples were sectioned into 50
810 nm slices using an ultramicrotome equipped with a diamond knife and mounted onto copper
811 grids suitable for TEM. The grids were stained with lead citrate for 3 minutes before imaging.
812 Images were captured using a Jeol 1400 Transmission Electron Microscope at magnifications
813 ranging from 800× to 1200× (digital magnification). Images were imported into ImageJ/Fiji to
814 quantify mitochondrial area, mitochondrial cristae density, and the number of
815 autophagosomes, autolysosomes, and lysosomes per field. Mitochondria and autophagic
816 vesicles were manually traced to determine the area.

817 **Quantification and statistical analysis**

818 All statistical analyses were performed using GraphPad Prism. For comparisons between two
819 groups, a two-tailed unpaired t-test was applied to normally distributed data. Multi-group
820 comparisons were analysed using one-way ANOVA followed by Tukey's multiple comparisons
821 test or two-way ANOVA. Data are presented as mean ± SEM. from at least three independent
822 replicates, with 50-70 cells per repeat for DA neurons and 10-15 cells per repeat for fibroblasts
823 for live cell imaging experiments. For immunoblotting or TMRM data, control sample means
824 were normalised to one to facilitate comparisons. Statistical significance was defined as

$p < 0.05$. p-values are reported as follows: *$p < 0.05$, **$p < 0.01$, ***$p < 0.005$, and ****$p < 0.001$, ns – not significant.

Acknowledgements

This project was funded by the Michael J Fox Foundation (Project number E27234 to MRD) and the Parkinson's UK Foundation (G-2103 to MRD and PS). The authors would also like to express their gratitude to the members of the Michael Duchen and Gyorgy Szabadkai labs for their feedback, as well as to students, including Shail Bhatt and Oriane Marguet, for their assistance with the preliminary data. We acknowledge the MRC Centre for Neuromuscular Diseases Biobank (supported by the National Institute for Health Research Biomedical Research Centres at Great Ormond Street Hospital for Children, NHS Foundation Trust) for providing the age- and sex-matched healthy controls and GBA1-E326K fibroblasts used in this study. Figure 6 was created using Biorender.com. We thank Dr. Elizabeth Slavik-Smith from the Electron Microscopy facility at UCL, Division of Biosciences, for her assistance with EM.

Author Contributions

P.S., M.R.D - Conceptualisation, funding acquisition, investigation, visualization, methodology, writing–original draft, project administration, writing–review and editing. A.C.B –methodology, investigation, visualisation and data analysis. S.K, A.F, I.K, K.S and T.S.B– Methodology, investigation and data analysis. O.S, J.Z and M.G – Resources.

Declaration of Interests

No competing interests in this research were declared by the authors.

References:

1. Baden P, Perez MJ, Raji H, Bertoli F, Kalb S, Illescas M, Spanos F, Giuliano C, Calogero AM, Oldrati M, Hebestreit H, Cappelletti G, Brockmann K, Gasser T, Schapira AHV, Ugalde C, Deleidi M (2023) Glucocerebrosidase is imported into mitochondria and preserves complex I integrity and energy metabolism. Nat Commun 14:1930. doi: 10.1038/s41467-023-37454-4

2. Bae E-J, Yang NY, Lee C, Lee H-J, Kim S, Sardi SP, Lee S-J (2015) Loss of glucocerebrosidase 1 activity causes lysosomal dysfunction and α-synuclein aggregation. Exp Mol Med 47:e153–e153. doi: 10.1038/emm.2014.128

3. Bindels DS, Haarbosch L, Van Weeren L, Postma M, Wiese KE, Mastop M, Aumonier S, Gotthard G, Royant A, Hink MA, Gadella TWJ (2017) mScarlet: a bright monomeric red fluorescent protein for cellular imaging. Nat Methods 14:53–56. doi: 10.1038/nmeth.4074

4. Blacker TS, Chen W, Avezov E, Marsh RJ, Duchen MR, Kaminski CF, Bain AJ (2017) Investigating State Restriction in Fluorescent Protein FRET Using Time-Resolved Fluorescence and Anisotropy. J Phys Chem C 121:1507–1514. doi: 10.1021/acs.jpcc.6b11235

5. Bourdenx M, Daniel J, Genin E, Soria FN, Blanchard-Desce M, Bezard E, Dehay B (2016) Nanoparticles restore lysosomal acidification defects: Implications for Parkinson and other lysosomal-related diseases. Autophagy 12:472–483. doi: 10.1080/15548627.2015.1136769

6. Boutagy NE, Rogers GW, Pyne ES, Ali MM, Hulver MW, Frisard MI (2015) Using Isolated Mitochondria from Minimal Quantities of Mouse Skeletal Muscle for High throughput Microplate Respiratory Measurements. J Vis Exp e53216. doi: 10.3791/53216

7. Burbulla LF, Jeon S, Zheng J, Song P, Silverman RB, Krainc D (2019) A modulator of wild-type glucocerebrosidase improves pathogenic phenotypes in dopaminergic neuronal models of Parkinson's disease. Sci Transl Med 11:eaau6870. doi: 10.1126/scitranslmed.aau6870

8. Byrns CN, Bonini NM (2021) An Integrated Multi-omics Approach Identifies Therapeutic Potential for ATP6V1A in Late Onset Alzheimer's Disease. Neuron 109:193–194. doi: 10.1016/j.neuron.2020.12.015

9. Capristo M, Del Dotto V, Tropeano CV, Fiorini C, Caporali L, La Morgia C, Valentino ML, Montopoli M, Carelli V, Maresca A (2022) Rapamycin rescues mitochondrial dysfunction in cells carrying the m.8344A > G mutation in the mitochondrial tRNALys. Mol Med 28:90. doi: 10.1186/s10020-022-00519-z

10. Carmona-Gutierrez D, Hughes AL, Madeo F, Ruckenstuhl C (2016) The crucial impact of lysosomes in aging and longevity. Ageing Research Reviews 32:2–12. doi: 10.1016/j.arr.2016.04.009

11. Chen L, Saito R, Noda-Narita S, Kassai H, Aiba A (2024) Hyperactive mTORC1 in striatum dysregulates dopamine receptor expression and odor preference behavior. Front Neurosci 18:1461178. doi: 10.3389/fnins.2024.1461178

12. Chin MY, Ang K-H, Davies J, Alquezar C, Garda VG, Rooney B, Leng K, Kampmann M, Arkin MR, Kao AW (2022) Phenotypic Screening Using High-Content Imaging to Identify Lysosomal pH Modulators in a Neuronal Cell Model. ACS Chem Neurosci 13:1505–1516. doi: 10.1021/acschemneuro.1c00804

13. Chung C-Y, Singh K, Sheshadri P, Valdebenito GE, Chacko AR, Costa Besada MA, Liang XF, Kabir L, Pitceathly RDS, Szabadkai G, Duchen MR (2024) Inhibition of the PI3K-AKT-MTORC1 axis reduces the burden of the m.3243A>G mtDNA mutation by promoting mitophagy and improving mitochondrial function. Autophagy 1–16. doi: 10.1080/15548627.2024.2437908

14. Coffey EE, Beckel JM, Laties AM, Mitchell CH (2014) Lysosomal alkalization and dysfunction in human fibroblasts with the Alzheimer's disease-linked presenilin 1 A246E mutation can be reversed with cAMP. Neuroscience 263:111–124. doi: 10.1016/j.neuroscience.2014.01.001

15. Croce AC, Bottiroli G (2014) Autofluorescence spectroscopy and imaging: a tool for biomedical research and diagnosis. Eur J Histochem. doi: 10.4081/ejh.2014.2461

16. De La Cruz López KG, Toledo Guzmán ME, Sánchez EO, García Carrancá A (2019) mTORC1 as a Regulator of Mitochondrial Functions and a Therapeutic Target in Cancer. Front Oncol 9:1373. doi: 10.3389/fonc.2019.01373

17. Dehay B, Martinez-Vicente M, Caldwell GA, Caldwell KA, Yue Z, Cookson MR, Klein C, Vila M, Bezard E (2013) Lysosomal impairment in Parkinson's disease. Movement Disorders 28:725–732. doi: 10.1002/mds.25462

18. Duran R, Mencacci NE, Angeli AV, Shoai M, Deas E, Houlden H, Mehta A, Hughes D, Cox TM, Deegan P, Schapira AH, Lees AJ, Limousin P, Jarman PR, Bhatia KP, Wood NW, Hardy J, Foltynie T (2013) The glucocerobrosidase E326K variant predisposes to Parkinson's disease, but does not cause Gaucher's disease. Movement Disorders 28:232–236. doi: 10.1002/mds.25248

19. Ebner M, Fröhlich F, Haucke V (2025) Mechanisms and functions of lysosomal lipid homeostasis. Cell Chemical Biology 32:392–407. doi: 10.1016/j.chembiol.2025.02.003

20. Falace A, Volpedo G, Scala M, Zara F, Striano P, Fassio A (2024) V-ATPase Dysfunction in the Brain: Genetic Insights and Therapeutic Opportunities. Cells 13:1441. doi: 10.3390/cells13171441

21. Fassio A, Esposito A, Kato M, Saitsu H, Mei D, Marini C, Conti V, Nakashima M, Okamoto N, Olmez Turker A, Albuz B, Semerci Gündüz CN, Yanagihara K, Belmonte E, Maragliano L, Ramsey K, Balak C, Siniard A, Narayanan V, C4RCD Research Group, Ohba C, Shiina M, Ogata K, Matsumoto N, Benfenati F, Guerrini R (2018) De novo mutations of the ATP6V1A gene cause developmental encephalopathy with epilepsy. Brain 141:1703–1718. doi: 10.1093/brain/awy092

22. Félix SS, O'Toole P, Oliveira NAS, Pinho BR, Blacker TS, Fernandes F, Oliveira JMA, Oroz J, Laurents DV, Cabrita EJ (2025) Pathological mutation in SMN impairs modulation of GAR1 phase separation linking condensate dysfunction to Spinal Muscular Atrophy

23. Furderer ML, Hertz E, Lopez GJ, Sidransky E (2022) Neuropathological Features of Gaucher Disease and Gaucher Disease with Parkinsonism. IJMS 23:5842. doi: 10.3390/ijms23105842

24. García-Sanz P, Orgaz L, Bueno-Gil G, Espadas I, Rodríguez-Traver E, Kulisevsky J, Gutierrez A, Dávila JC, González-Polo RA, Fuentes JM, Mir P, Vicario C, Moratalla R (2017) N370S -*GBA1* mutation causes lysosomal cholesterol accumulation in Parkinson's disease. Movement Disorders 32:1409–1422. doi: 10.1002/mds.27119

25. Gegg ME, Schapira AHV (2016) Mitochondrial dysfunction associated with glucocerebrosidase deficiency. Neurobiology of Disease 90:43–50. doi: 10.1016/j.nbd.2015.09.006

26. Guerrini R, Mei D, Kerti-Szigeti K, Pepe S, Koenig MK, Von Allmen G, Cho MT, McDonald K, Baker J, Bhambhani V, Powis Z, Rodan L, Nabbout R, Barcia G, Rosenfeld JA, Bacino CA, Mignot C, Power LH, Harris CJ, Marjanovic D, Møller RS, Hammer TB, The DDD Study, Keski Filppula R, Vieira P, Hildebrandt C, Sacharow S, Undiagnosed Diseases Network, Maragliano L, Benfenati F, Lachlan K, Benneche A, Petit F, De Sainte Agathe JM, Hallinan B, Si Y, Wentzensen IM, Zou F, Narayanan V, Matsumoto N, Boncristiano A, La Marca G, Kato M, Anderson K, Barba C, Sturiale L, Garozzo D, Bei R, ATP6V1A collaborators, Masuelli L, Conti V, Novarino G, Fassio A (2022) Phenotypic and genetic spectrum of ATP6V1A encephalopathy: a disorder of lysosomal homeostasis. Brain 145:2687–2703. doi: 10.1093/brain/awac145

27. Haltia M, Goebel HH (2013) The neuronal ceroid-lipofuscinoses: A historical introduction. Biochimica et Biophysica Acta (BBA) - Molecular Basis of Disease 1832:1795–1800. doi: 10.1016/j.bbadis.2012.08.012

28. Henrich MT, Oertel WH, Surmeier DJ, Geibl FF (2023) Mitochondrial dysfunction in Parkinson's disease – a key disease hallmark with therapeutic potential. Mol Neurodegeneration 18:83. doi: 10.1186/s13024-023-00676-7

29. Hosios AM, Wilkinson ME, McNamara MC, Kalafut KC, Torrence ME, Asara JM, Manning BD (2022) mTORC1 regulates a lysosome-dependent adaptive shift in intracellular lipid species. Nat Metab 4:1792–1811. doi: 10.1038/s42255-022-00706-6

30. Im E, Jiang Y, Stavrides PH, Darji S, Erdjument-Bromage H, Neubert TA, Choi JY, Wegiel J, Lee J-H, Nixon RA (2023) Lysosomal dysfunction in Down syndrome and Alzheimer mouse models is caused by v-ATPase inhibition by Tyr^{682} -phosphorylated APP βCTF. Sci Adv 9:eadg1925. doi: 10.1126/sciadv.adg1925

31. Kilpatrick BS, Magalhaes J, Beavan MS, McNeill A, Gegg ME, Cleeter MWJ, Bloor-Young D, Churchill GC, Duchen MR, Schapira AH, Patel S (2016) Endoplasmic reticulum and lysosomal Ca2+ stores are remodelled in GBA1-linked Parkinson disease patient fibroblasts. Cell Calcium 59:12–20. doi: 10.1016/j.ceca.2015.11.002

32. Kim S, Wong YC, Gao F, Krainc D (2021) Dysregulation of mitochondria-lysosome contacts by GBA1 dysfunction in dopaminergic neuronal models of Parkinson's disease. Nat Commun 12:1807. doi: 10.1038/s41467-021-22113-3

971 33. Kim S-H, Cho Y-S, Kim Y, Park J, Yoo S-M, Gwak J, Kim Y, Gwon Y, Kam T, Jung Y-K
972 (2023) Endolysosomal impairment by binding of amyloid beta or MAPT/Tau to V-ATPase
973 and rescue via the HYAL-CD44 axis in Alzheimer disease. Autophagy 19:2318–2337.
974 doi: 10.1080/15548627.2023.2181614

975 34. Lawrence RE, Zoncu R (2019) The lysosome as a cellular centre for signalling,
976 metabolism and quality control. Nat Cell Biol 21:133–142. doi: 10.1038/s41556-018-
977 0244-7

978 35. Li H, Ham A, Ma TC, Kuo S-H, Kanter E, Kim D, Ko HS, Quan Y, Sardi SP, Li A, Arancio
979 O, Kang UJ, Sulzer D, Tang G (2019) Mitochondrial dysfunction and mitophagy defect
980 triggered by heterozygous *GBA* mutations. Autophagy 15:113–130. doi:
981 10.1080/15548627.2018.1509818

982 36. Lipton JO, Sahin M (2014) The Neurology of mTOR. Neuron 84:275–291. doi:
983 10.1016/j.neuron.2014.09.034

984 37. Liu X, Li Y, Yu L, Vickstrom CR, Liu Q (2018) VTA mTOR Signaling Regulates
985 Dopamine Dynamics, Cocaine-Induced Synaptic Alterations, and Reward.
986 Neuropsychopharmacol 43:1066–1077. doi: 10.1038/npp.2017.247

987 38. Liu Z, Zhuang W, Cai M, Lv E, Wang Y, Wu Z, Wang H, Fu W (2022) Kaemperfol
988 Protects Dopaminergic Neurons by Promoting mTOR-Mediated Autophagy in
989 Parkinson's Disease Models. Neurochem Res. doi: 10.1007/s11064-022-03819-2

990 39. Lwin A (2004) Glucocerebrosidase mutations in subjects with parkinsonism. Molecular
991 Genetics and Metabolism 81:70–73. doi: 10.1016/j.ymgme.2003.11.004

992 40. Magalhaes J, Gegg ME, Migdalska-Richards A, Doherty MK, Whitfield PD, Schapira
993 AHV (2016) Autophagic lysosome reformation dysfunction in glucocerebrosidase
994 deficient cells: relevance to Parkinson disease. Hum Mol Genet 25:3432–3445. doi:
995 10.1093/hmg/ddw185

996 41. Masters TA, Marsh RJ, Armoogum DA, Nicolaou N, Larijani B, Bain AJ (2013)
997 Restricted State Selection in Fluorescent Protein Förster Resonance Energy Transfer. J
998 Am Chem Soc 135:7883–7890. doi: 10.1021/ja312230b

999 42. Matassini C, Warren J, Wang B, Goti A, Cardona F, Morrone A, Bols M (2020) Imino-
1000 and Azasugar Protonation Inside Human Acid β-Glucosidase, the Enzyme that is
1001 Defective in Gaucher Disease. Angew Chem Int Ed 59:10466–10469. doi:
1002 10.1002/anie.202002850

1003 43. Mauvezin C, Nagy P, Juhász G, Neufeld TP (2015) Autophagosome–lysosome fusion is
1004 independent of V-ATPase-mediated acidification. Nat Commun 6:7007. doi:
1005 10.1038/ncomms8007

1006 44. Merrill RA, Flippo KH, Strack S (2017) Measuring Mitochondrial Shape with ImageJ.
1007 In: Strack S, Usachev YM (eds) Techniques to Investigate Mitochondrial Function in
1008 Neurons. Springer New York, New York, NY, pp 31–48

1009 45. Morita M, Gravel S-P, Hulea L, Larsson O, Pollak M, St-Pierre J, Topisirovic I (2015)
1010 mTOR coordinates protein synthesis, mitochondrial activity and proliferation. Cell Cycle
1011 14:473–480. doi: 10.4161/15384101.2014.991572

1012 46. Navarro-Romero A, Fernandez-Gonzalez I, Riera J, Montpeyo M, Albert-Bayo M, Lopez-
1013 Royo T, Castillo-Sanchez P, Carnicer-Caceres C, Arranz-Amo JA, Castillo-Ribelles L,
1014 Pradas E, Casas J, Vila M, Martinez-Vicente M (2022) Lysosomal lipid alterations caused
1015 by glucocerebrosidase deficiency promote lysosomal dysfunction, chaperone-mediated-
1016 autophagy deficiency, and alpha-synuclein pathology. npj Parkinsons Dis 8:126. doi:
1017 10.1038/s41531-022-00397-6

1018 47. Neikirk K, Vue Z, Katti P, Rodriguez BI, Omer S, Shao J, Christensen T, Garza Lopez E,
1019 Marshall A, Palavicino-Maggio CB, Ponce J, Alghanem AF, Vang L, Barongan T, Beasley
1020 HK, Rodman T, Stephens D, Mungai M, Correia M, Exil V, Damo S, Murray SA, Crabtree
1021 A, Glancy B, Pereira RO, Abel ED, Hinton AO (2023) Systematic Transmission Electron
1022 Microscopy-Based Identification and 3D Reconstruction of Cellular Degradation
1023 Machinery. Advanced Biology 7:2200221. doi: 10.1002/adbi.202200221

1024 48. Offman MN, Krol M, Silman I, Sussman JL, Futerman AH (2010) Molecular Basis of
1025 Reduced Glucosylceramidase Activity in the Most Common Gaucher Disease Mutant,
1026 N370S. Journal of Biological Chemistry 285:42105–42114. doi:
1027 10.1074/jbc.M110.172098

1028 49. Osellame LD, Rahim AA, Hargreaves IP, Gegg ME, Richard-Londt A, Brandner S,
1029 Waddington SN, Schapira AHV, Duchen MR (2013) Mitochondria and Quality Control
1030 Defects in a Mouse Model of Gaucher Disease—Links to Parkinson's Disease. Cell
1031 Metabolism 17:941–953. doi: 10.1016/j.cmet.2013.04.014

1032 50. Pietrafesa D, Casamassa A, Benassi B, Santoro M, Marano M, Consales C, Rosati J,
1033 Arcangeli C (2024) Investigating the Impact of the Parkinson's-Associated GBA1 E326K
1034 Mutation on β-Glucocerebrosidase Dimerization and Interactome Dynamics Through an
1035 In Silico Approach. IJMS 25:11443. doi: 10.3390/ijms252111443

1036 51. Pitcairn C, Wani WY, Mazzulli JR (2019) Dysregulation of the autophagic-lysosomal
1037 pathway in Gaucher and Parkinson's disease. Neurobiology of Disease 122:72–82. doi:
1038 10.1016/j.nbd.2018.03.008

1039 52. Ponsford AH, Ryan TA, Raimondi A, Cocucci E, Wycislo SA, Fröhlich F, Swan LE, Stagi
1040 M (2021) Live imaging of intra-lysosome pH in cell lines and primary neuronal culture
1041 using a novel genetically encoded biosensor. Autophagy 17:1500–1518. doi:
1042 10.1080/15548627.2020.1771858

1043 53. Ratto E, Chowdhury SR, Siefert NS, Schneider M, Wittmann M, Helm D, Palm W (2022)
1044 Direct control of lysosomal catabolic activity by mTORC1 through regulation of V-
1045 ATPase assembly. Nat Commun 13:4848. doi: 10.1038/s41467-022-32515-6

1046 54. Rubilar JC, Outeiro TF, Klein AD (2024) The lysosomal β-glucocerebrosidase strikes
1047 mitochondria: implications for Parkinson's therapeutics. Brain 147:2610–2620. doi:
1048 10.1093/brain/awae070

1049 55. Rujano MA, Cannata Serio M, Panasyuk G, Péanne R, Reunert J, Rymen D, Hauser V,
1050 Park JH, Freisinger P, Souche E, Guida MC, Maier EM, Wada Y, Jäger S, Krogan NJ,
1051 Kretz O, Nobre S, Garcia P, Quelhas D, Bird TD, Raskind WH, Schwake M, Duvet S,
1052 Foulquier F, Matthijs G, Marquardt T, Simons M (2017) Mutations in the X-linked
1053 *ATP6AP2* cause a glycosylation disorder with autophagic defects. Journal of
1054 Experimental Medicine 214:3707–3729. doi: 10.1084/jem.20170453

1055 56. Sabers CJ, Martin MM, Brunn GJ, Williams JM, Dumont FJ, Wiederrecht G, Abraham
1056 RT (1995) Isolation of a Protein Target of the FKBP12-Rapamycin Complex in
1057 Mammalian Cells. Journal of Biological Chemistry 270:815–822. doi:
1058 10.1074/jbc.270.2.815

1059 57. Salvioli R, Tatti M, Scarpa S, Moavero SM, Ciaffoni F, Felicetti F, Kaneski CR, Brady
1060 RO, Vaccaro AM (2005) The N370S (Asn370→Ser) mutation affects the capacity of
1061 glucosylceramidase to interact with anionic phospholipid-containing membranes and
1062 saposin C. Biochemical Journal 390:95–103. doi: 10.1042/BJ20050325

1063 58. Schöndorf DC, Aureli M, McAllister FE, Hindley CJ, Mayer F, Schmid B, Sardi SP,
1064 Valsecchi M, Hoffmann S, Schwarz LK, Hedrich U, Berg D, Shihabuddin LS, Hu J,
1065 Pruszak J, Gygi SP, Sonnino S, Gasser T, Deleidi M (2014) iPSC-derived neurons from
1066 GBA1-associated Parkinson's disease patients show autophagic defects and impaired
1067 calcium homeostasis. Nat Commun 5:4028. doi: 10.1038/ncomms5028

1068 59. Settembre C, Fraldi A, Medina DL, Ballabio A (2013) Signals from the lysosome: a
1069 control centre for cellular clearance and energy metabolism. Nat Rev Mol Cell Biol
1070 14:283–296. doi: 10.1038/nrm3565

1071 60. Sidransky E, Nalls MA, Aasly JO, Aharon-Peretz J, Annesi G, Barbosa ER, Bar-Shira A,
1072 Berg D, Bras J, Brice A, Chen C-M, Clark LN, Condroyer C, De Marco EV, Dürr A, Eblan
1073 MJ, Fahn S, Farrer MJ, Fung H-C, Gan-Or Z, Gasser T, Gershoni-Baruch R, Giladi N,
1074 Griffith A, Gurevich T, Januario C, Kropp P, Lang AE, Lee-Chen G-J, Lesage S, Marder
1075 K, Mata IF, Mirelman A, Mitsui J, Mizuta I, Nicoletti G, Oliveira C, Ottman R, Orr-
1076 Urtreger A, Pereira LV, Quattrone A, Rogaeva E, Rolfs A, Rosenbaum H, Rozenberg R,
1077 Samii A, Samaddar T, Schulte C, Sharma M, Singleton A, Spitz M, Tan E-K, Tayebi N,
1078 Toda T, Troiano AR, Tsuji S, Wittstock M, Wolfsberg TG, Wu Y-R, Zabetian CP, Zhao Y,
1079 Ziegler SG (2009) Multicenter Analysis of Glucocerebrosidase Mutations in Parkinson's
1080 Disease. N Engl J Med 361:1651–1661. doi: 10.1056/NEJMoa0901281

1081 61. Sillence DJ (2013) Glucosylceramide modulates endolysosomal pH in Gaucher disease.
1082 Molecular Genetics and Metabolism 109:194–200. doi: 10.1016/j.ymgme.2013.03.015

1083 62. Singh K, Duchen MR (2022) Analysis of Organization and Activity of Mitochondrial
1084 Respiratory Chain Complexes in Primary Fibroblasts Using Blue Native PAGE. Methods
1085 Mol Biol 2497:339–348. doi: 10.1007/978-1-0716-2309-1_25

1086 63. Song Q, Meng B, Xu H, Mao Z (2020) The emerging roles of vacuolar-type ATPase-
1087 dependent Lysosomal acidification in neurodegenerative diseases. Transl Neurodegener
1088 9:17. doi: 10.1186/s40035-020-00196-0

64. Song SB, Shim W, Hwang ES (2023) Lipofuscin Granule Accumulation Requires Autophagy Activation. Molecules and Cells 46:486–495. doi: 10.14348/molcells.2023.0019

65. Steet RA, Chung S, Wustman B, Powe A, Do H, Kornfeld SA (2006) The iminosugar isofagomine increases the activity of N370S mutant acid β-glucosidase in Gaucher fibroblasts by several mechanisms. Proc Natl Acad Sci USA 103:13813–13818. doi: 10.1073/pnas.0605928103

66. Suhling K, Hirvonen LM, Levitt JA, Chung P-H, Tregidgo C, Le Marois A, Rusakov DA, Zheng K, Ameer-Beg S, Poland S, Coelho S, Henderson R, Krstajic N (2015) Fluorescence lifetime imaging (FLIM): Basic concepts and some recent developments. Medical Photonics 27:3–40. doi: 10.1016/j.medpho.2014.12.001

67. Sun N, Malide D, Liu J, Rovira II, Combs CA, Finkel T (2017) A fluorescence-based imaging method to measure in vitro and in vivo mitophagy using mt-Keima. Nat Protoc 12:1576–1587. doi: 10.1038/nprot.2017.060

68. Tintos-Hernández JA, Santana A, Keller KN, Ortiz-González XR (2021) Lysosomal dysfunction impairs mitochondrial quality control and is associated with neurodegeneration in *TBCK* encephaloneuronopathy. Brain Communications 3:fcab215. doi: 10.1093/braincomms/fcab215

69. Virdi GS, Choi ML, Evans JR, Yao Z, Athauda D, Strohbuecker S, Nirujogi RS, Wernick AI, Pelegrina-Hidalgo N, Leighton C, Saleeb RS, Kopach O, Alrashidi H, Melandri D, Perez-Lloret J, Angelova PR, Sylantyev S, Eaton S, Heales S, Rusakov DA, Alessi DR, Kunath T, Horrocks MH, Abramov AY, Patani R, Gandhi S (2022) Protein aggregation and calcium dysregulation are hallmarks of familial Parkinson's disease in midbrain dopaminergic neurons. npj Parkinsons Dis 8:162. doi: 10.1038/s41531-022-00423-7

70. Wang M, Li A, Sekiya M, Beckmann ND, Quan X, Schrode N, Fernando MB, Yu A, Zhu L, Cao J, Lyu L, Horgusluoglu E, Wang Q, Guo L, Wang Y, Neff R, Song W, Wang E, Shen Q, Zhou X, Ming C, Ho S-M, Vatansever S, Kaniskan HÜ, Jin J, Zhou M-M, Ando K, Ho L, Slesinger PA, Yue Z, Zhu J, Katsel P, Gandy S, Ehrlich ME, Fossati V, Noggle S, Cai D, Haroutunian V, Iijima KM, Schadt E, Brennand KJ, Zhang B (2021) Transformative Network Modeling of Multi-omics Data Reveals Detailed Circuits, Key Regulators, and Potential Therapeutics for Alzheimer's Disease. Neuron 109:257-272.e14. doi: 10.1016/j.neuron.2020.11.002

71. Wei RR, Hughes H, Boucher S, Bird JJ, Guziewicz N, Van Patten SM, Qiu H, Pan CQ, Edmunds T (2011) X-ray and Biochemical Analysis of N370S Mutant Human Acid β-Glucosidase. Journal of Biological Chemistry 286:299–308. doi: 10.1074/jbc.M110.150433

72. Yates SC, Zafar A, Hubbard P, Nagy S, Durant S, Bicknell R, Wilcock G, Christie S, Esiri MM, Smith AD, Nagy Z (2013) Dysfunction of the mTOR pathway is a risk factor for Alzheimer's disease. acta neuropathol commun 1:3. doi: 10.1186/2051-5960-1-3

73. Zeng J, Acin-Perez R, Assali EA, Martin A, Brownstein AJ, Petcherski A, Fernández-del-Rio L, Xiao R, Lo CH, Shum M, Liesa M, Han X, Shirihai OS, Grinstaff MW (2023) Restoration of lysosomal acidification rescues autophagy and metabolic dysfunction in

1131 non-alcoholic fatty liver disease. Nat Commun 14:2573. doi: 10.1038/s41467-023-38165-
1132 6

1133 74. Zhang J, Zeng W, Han Y, Lee W-R, Liou J, Jiang Y (2023) Lysosomal LAMP proteins
1134 regulate lysosomal pH by direct inhibition of the TMEM175 channel. Molecular Cell
1135 83:2524-2539.e7. doi: 10.1016/j.molcel.2023.06.004

1136 75. Zheng W, Li K, Zhong M, Wu K, Zhou L, Huang J, Liu L, Chen Z (2024) Mitophagy
1137 activation by rapamycin enhances mitochondrial function and cognition in 5×FAD mice.
1138 Behavioural Brain Research 463:114889. doi: 10.1016/j.bbr.2024.114889

1139

1140 **Table 1 – List of cell lines used**

Cell Lines used	Cell Line ID	Age/Sex	Cell type	Mutation	Source	Ethics Committee Approval
CONTROL 1	CONTROL 1	77/Male	Fibroblasts	No Mutation	NHNN	PD Royal Free Ethics
N370S	ND34263	65/Male	Fibroblasts; source for NH50182 iPSCs	GBA1-N370S; Heterozygous	NIH-RUCDR	
CONTROL 2	CONTROL 2	55/Male	Fibroblasts; source for Control1 iPSCs	No Mutation	NHNN	PD Royal Free Ethics
E326K 1	Het1/ JS48753	58/Male	Fibroblasts; source for Het1/E326K 1 iPSCs	GBA1-E326K; Heterozygous	NHNN	PD Royal Free Ethics
E326K 2	ND41015	63/Male	Fibroblasts; source for ND50045 iPSCs	GBA1-E326K; Heterozygous	NIH-RUCDR	
Isogenic Control (IsoC)	NH50142	63/Male	iPSCs; Isogenic Control for ND50045	CRISPR corrected GBA1-E326K heterozygous mutation	NIH-RUCDR	
E326K	ND50045	63/Male	iPSCs	GBA1-E326K; Heterozygous	NIH-RUCDR	
Isogenic Control (IsoC)	NH50186	65/Male	iPSCs; Isogenic Control for NH50182	CRISPR corrected GBA1-N370S heterozygous mutation	NIH-RUCDR	
N370S	NH50182	65/Male	iPSCs	GBA1-N370S; Heterozygous	NIH-RUCDR	
Control	Control 1	55/Male	iPSCs	No Mutation	Derived from CONTROL 2 fibroblasts	PD Royal Free Ethics for CONTROL 2 fibroblasts
E326K 1	Het1/ JS48753	58/Male	iPSCs	GBA1-E326K; Heterozygous	Derived from Het1 fibroblasts	PD Royal Free Ethics

						for JS48753 fibroblasts
E326K 2	Het 2/ MB240649	63/Male	iPSCs	GBA1-E326K; Heterozygous	Derived from MB240649 fibroblasts	PD Royal Free Ethics (for MB240649 fibroblasts
Control	SFC156 (Control 2)	65/Male	iPSCs	No Mutation	EBiSC	
N370S 1	SFC834 (N370S1)	72/Male	iPSCs	GBA1-N370S; Heterozygous	EBiSC	
N370S 2	SFC848 (N370S2)	68/Male	iPSCs	GBA1-N370S; Heterozygous	EBiSC	

1141

1142 **Table 2 : List of antibodies used in the study**

Name	Catalogue no.	Host	Company	Application	Concentration
ATP6V0D2	AB194557	Mouse	Abcam	Western Blotting	1:1000
LAMP1 (H4A3)	sc-20011	Mouse	Santa Cruz	Western Blotting, Immunofluorescence	1:500
GBA (c-term)	64171	Rabbit	Sigma	Western Blotting	1:700
ATP6V1H	AB187706	Rabbit	Abcam	Western Blotting	1:1000
ATP6V1A	199326	Rabbit	Abcam	Western Blotting	1:1000
pMTOR	55365	Rabbit	Abcam	Western Blotting	1:1000
MTOR	45175	Mouse	Cell Signalling	Western Blotting	1:1000
ATG5 (D5F5U)	12994T	Rabbit	Cell Signalling	Western Blotting	1:1000
P62	610833	Mouse	BD Biosystems	Western Blotting	1:1000
LC3	L7543	Rabbit	Sigma	Western Blotting	1:1000
B-ACTIN	ab8226	Mouse	Cell Signalling	Western Blotting	1:5000
TOM20	ab186735	Rabbit	Abcam	Western Blotting	1:1000
LC3	PM036	Rabbit	MBL Biosystems	Immunofluorescence	1:500
Citrate Synthetase	ab96600	Rabbit	Abcam	Immunofluorescence	1:200
OXPHOS Cocktail	45-8199	Mouse	Thermoscientific	Western Blotting	1:1000
Alexa Fluor 488	A-11008	Goat	Thermoscientific	Immunofluorescence	1:1000
Alexa Fluor 594	A-11012	Goat	Thermoscientific	Immunofluorescence	1:1000
Alexa Fluor 647	A-21235	Goat	Thermoscientific	Immunofluorescence	1:1000
IRDye® 680RD Goat anti-Mouse	926-68070	Goat	Li-COR Biosciences	Western Blotting	1:10000
IRDye® 800CW Goat anti-Rabbit IgG	926-32211	Goat	Li-COR Biosciences	Western Blotting	1:10000

1143

1144

1145

Figure 1

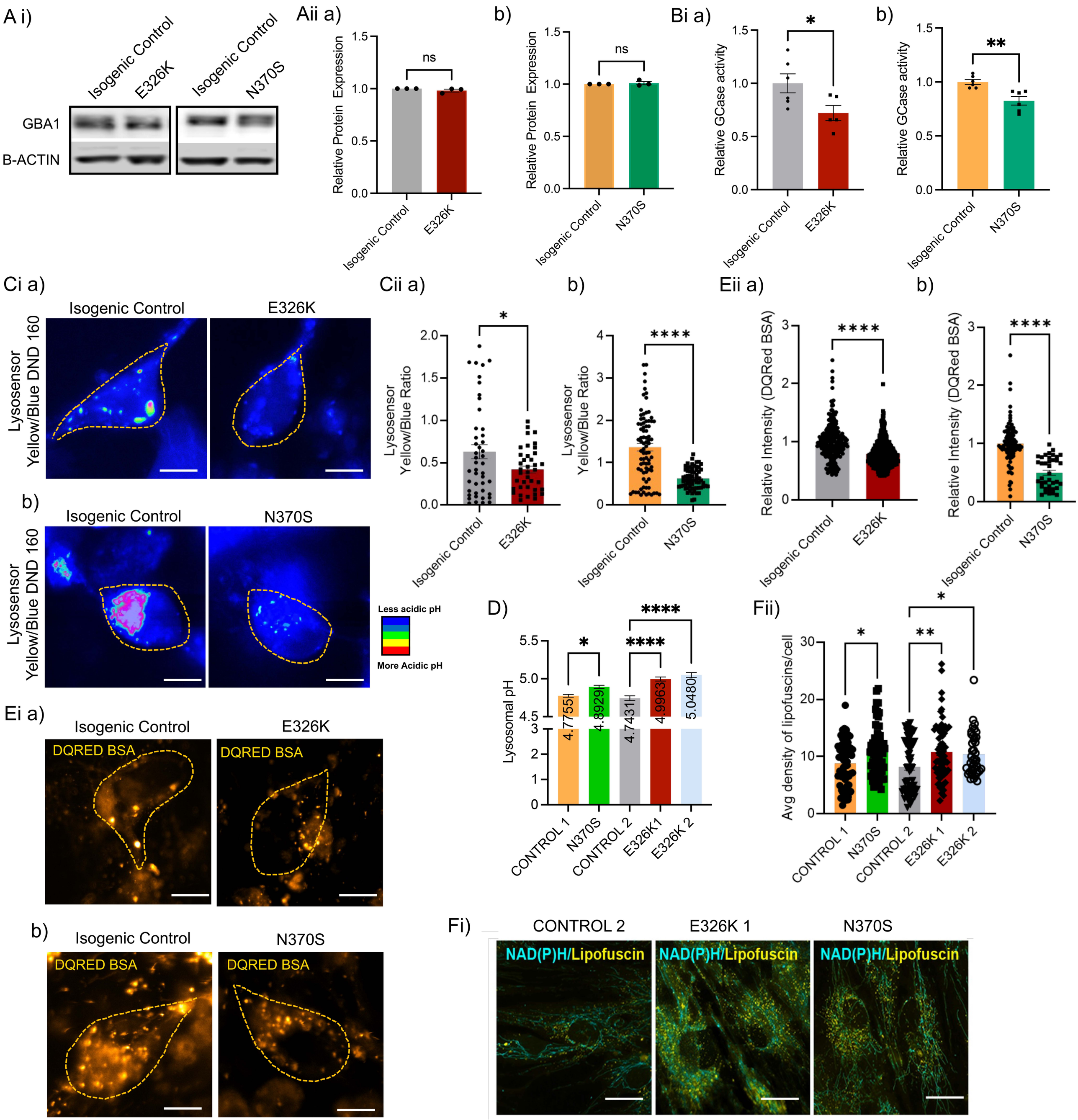
A i)
Isogenic Control
E326K
Isogenic Control
N370S
GBA1
B-ACTIN
Aii a)
Relative Protein Expression
ns
Isogenic Control
E326K
b)
Relative Protein Expression
ns
Isogenic Control
N370S
Bi a)
Relative GCase activity
*
Isogenic Control
E326K
b)
Relative GCase activity
**
Isogenic Control
N370S
Ci a)
Isogenic Control
E326K
Lysosensor Yellow/Blue DND 160
b)
Isogenic Control
N370S
Lysosensor Yellow/Blue DND 160
Less acidic pH
More Acidic pH
Cii a)
Lysosensor Yellow/Blue Ratio
*
Isogenic Control
E326K
b)
Lysosensor Yellow/Blue Ratio
****
Isogenic Control
N370S
Eii a)
Relative Intensity (DQRed BSA)
****
Isogenic Control
E326K
b)
Relative Intensity (DQRed BSA)
****
Isogenic Control
N370S
Ei a)
Isogenic Control
E326K
DQRED BSA
DQRED BSA
b)
Isogenic Control
N370S
DQRED BSA
DQRED BSA
D)
Lysosomal pH
*
****
****
4.7755
4.8929
4.7431
4.9963
5.0480
CONTROL 1
N370S
CONTROL 2
E326K1
E326K 2
Fii)
Avg density of lipofuscins/cell
*
**
*
CONTROL 1
N370S
CONTROL 2
E326K 1
E326K 2
Fi)
CONTROL 2
E326K 1
N370S
NAD(P)H/Lipofuscin
NAD(P)H/Lipofuscin
NAD(P)H/Lipofuscin

Figure 2

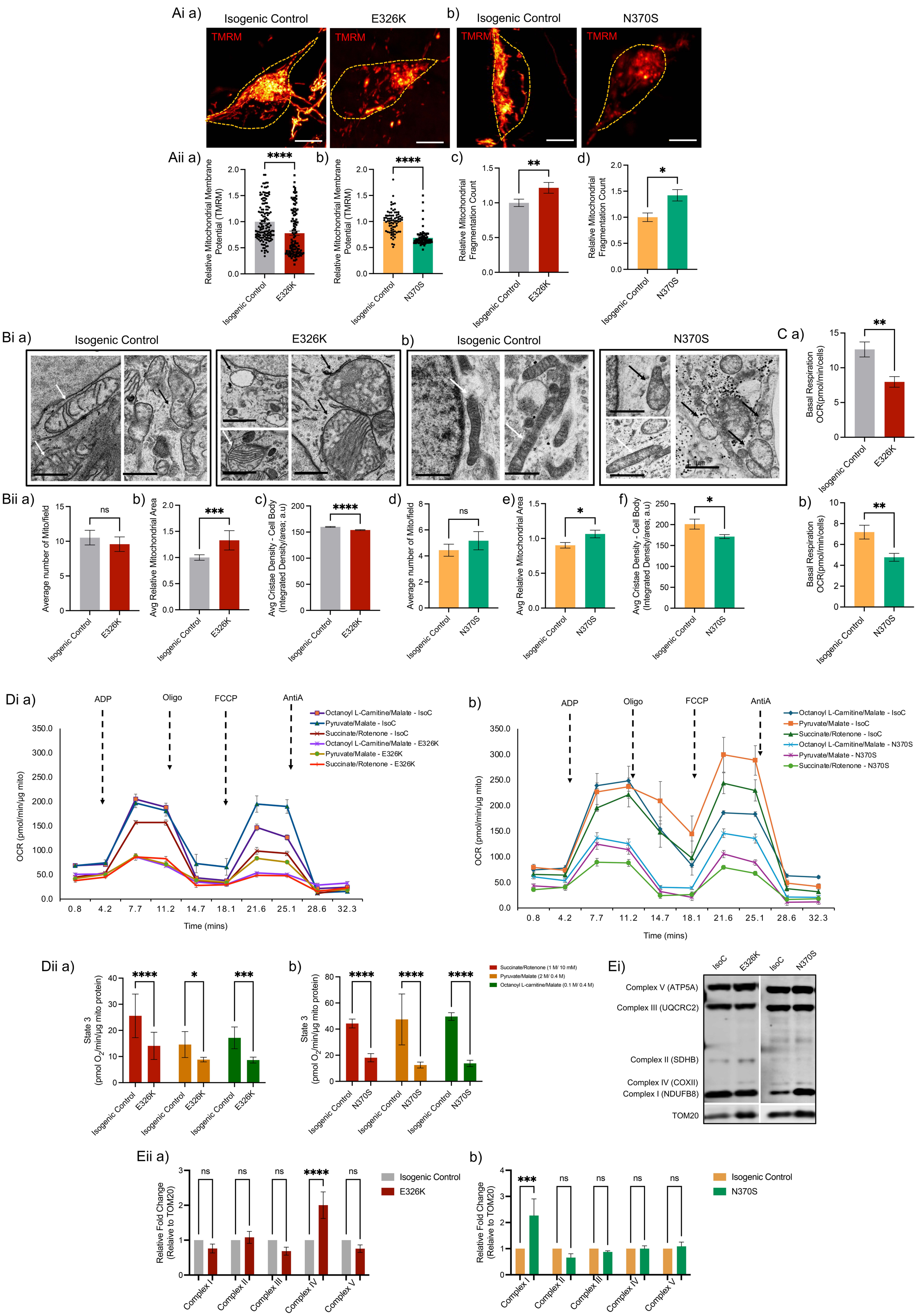
Ai a)
Isogenic Control
E326K
b)
Isogenic Control
N370S
TMRM
Aii a)
Relative Mitochondrial Membrane Potential (TMRM)
****
b)
Relative Mitochondrial Membrane Potential (TMRM)
****
c)
Relative Mitochondrial Fragmentation Count
**
d)
Relative Mitochondrial Fragmentation Count
*
Isogenic Control
E326K
N370S
Bi a)
Isogenic Control
E326K
b)
Isogenic Control
N370S
C a)
Basal Respiration OCR(pmol/min/cells)
**
Bii a)
Average number of Mito/field
ns
b)
Avg Relative Mitochondrial Area
***
c)
Avg Cristae Density - Cell Body (Integrated Density/area; a.u)
****
d)
Average number of Mito/field
ns
e)
Avg Relative Mitochondrial Area
*
f)
Avg Cristae Density - Cell Body (Integrated Density/area; a.u)
*
b)
Basal Respiration OCR(pmol/min/cells)
**
Di a)
ADP
Oligo
FCCP
AntiA
Octanoyl L-Carnitine/Malate - IsoC
Pyruvate/Malate - IsoC
Succinate/Rotenone - IsoC
Octanoyl L-Carnitine/Malate - E326K
Pyruvate/Malate - E326K
Succinate/Rotenone - E326K
OCR (pmol/min/µg mito)
Time (mins)
b)
Octanoyl L-Carnitine/Malate - N370S
Pyruvate/Malate - N370S
Succinate/Rotenone - N370S
Dii a)
State 3 (pmol O2/min/µg mito protein)
Succinate/Rotenone (1 M/ 10 mM)
Pyruvate/Malate (2 M/ 0.4 M)
Octanoyl L-carnitine/Malate (0.1 M/ 0.4 M)
Ei)
IsoC
E326K
N370S
Complex V (ATP5A)
Complex III (UQCRC2)
Complex II (SDHB)
Complex IV (COXII)
Complex I (NDUFB8)
TOM20
Eii a)
Relative Fold Change (Relative to TOM20)
Complex I
Complex II
Complex III
Complex IV
Complex V
Isogenic Control
E326K
b)
N370S

Figure 3

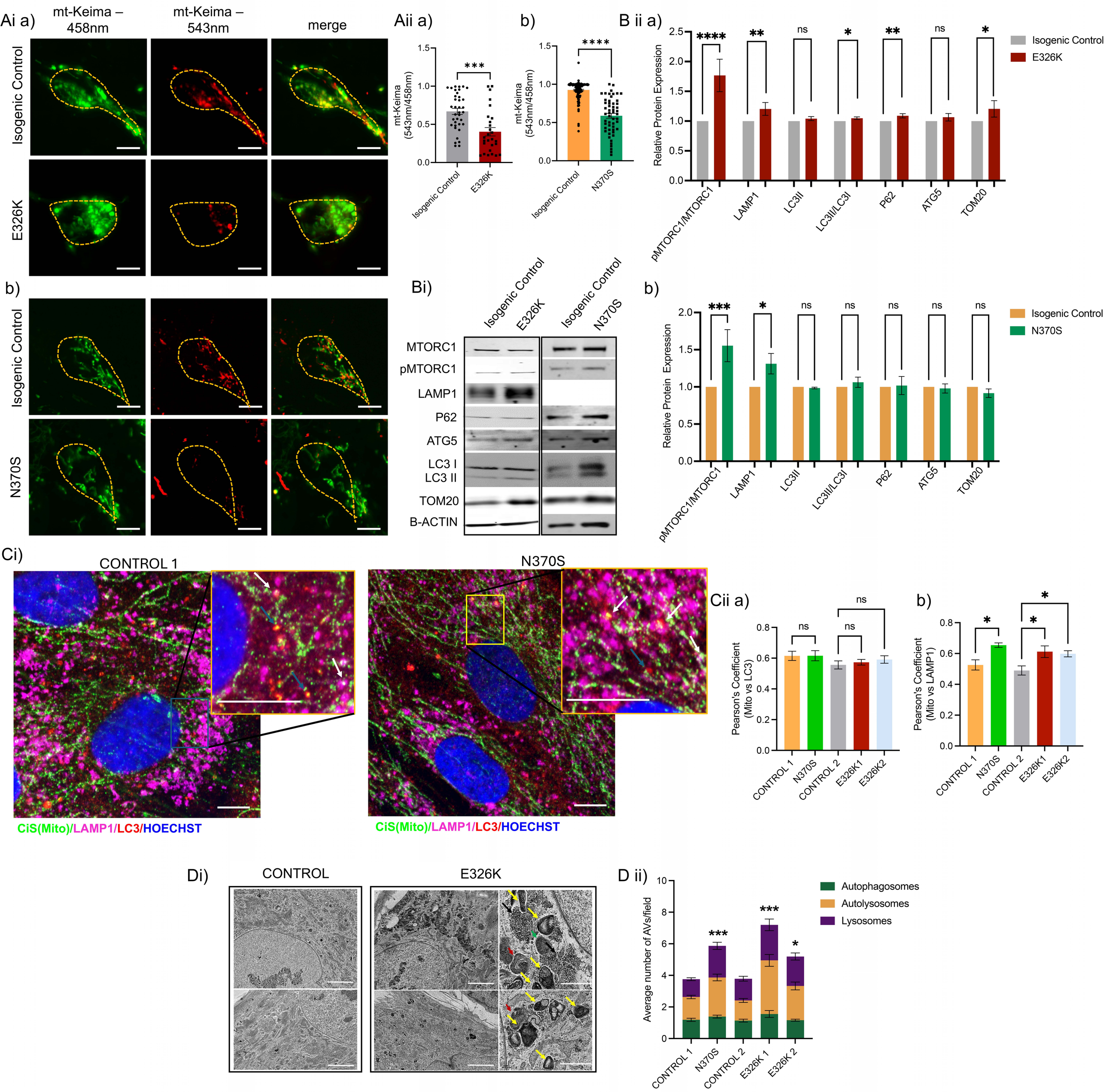
Ai a)
mt-Keima – 458nm
mt-Keima – 543nm
merge
Isogenic Control
E326K
b)
Isogenic Control
N370S
Aii a)
mt-Keima (543nm/458nm)
***
Isogenic Control
E326K
b)
****
Isogenic Control
N370S
B ii a)
Relative Protein Expression
****
**
ns
*
**
ns
*
Isogenic Control
E326K
pMTORC1/MTORC1
LAMP1
LC3II
LC3II/LC3I
P62
ATG5
TOM20
Bi)
Isogenic Control
E326K
Isogenic Control
N370S
MTORC1
pMTORC1
LAMP1
P62
ATG5
LC3 I
LC3 II
TOM20
B-ACTIN
b)
Relative Protein Expression
***
*
ns
Isogenic Control
N370S
Ci)
CONTROL 1
N370S
CiS(Mito)/LAMP1/LC3/HOECHST
CiS(Mito)/LAMP1/LC3/HOECHST
Cii a)
Pearson's Coefficient (Mito vs LC3)
ns
CONTROL 1
N370S
CONTROL 2
E326K1
E326K2
b)
Pearson's Coefficient (Mito vs LAMP1)
*
CONTROL 1
N370S
CONTROL 2
E326K1
E326K2
Di)
CONTROL
E326K
D ii)
Average number of AVs/field
***
*
Autophagosomes
Autolysosomes
Lysosomes
CONTROL 1
N370S
CONTROL 2
E326K 1
E326K 2

Figure 4

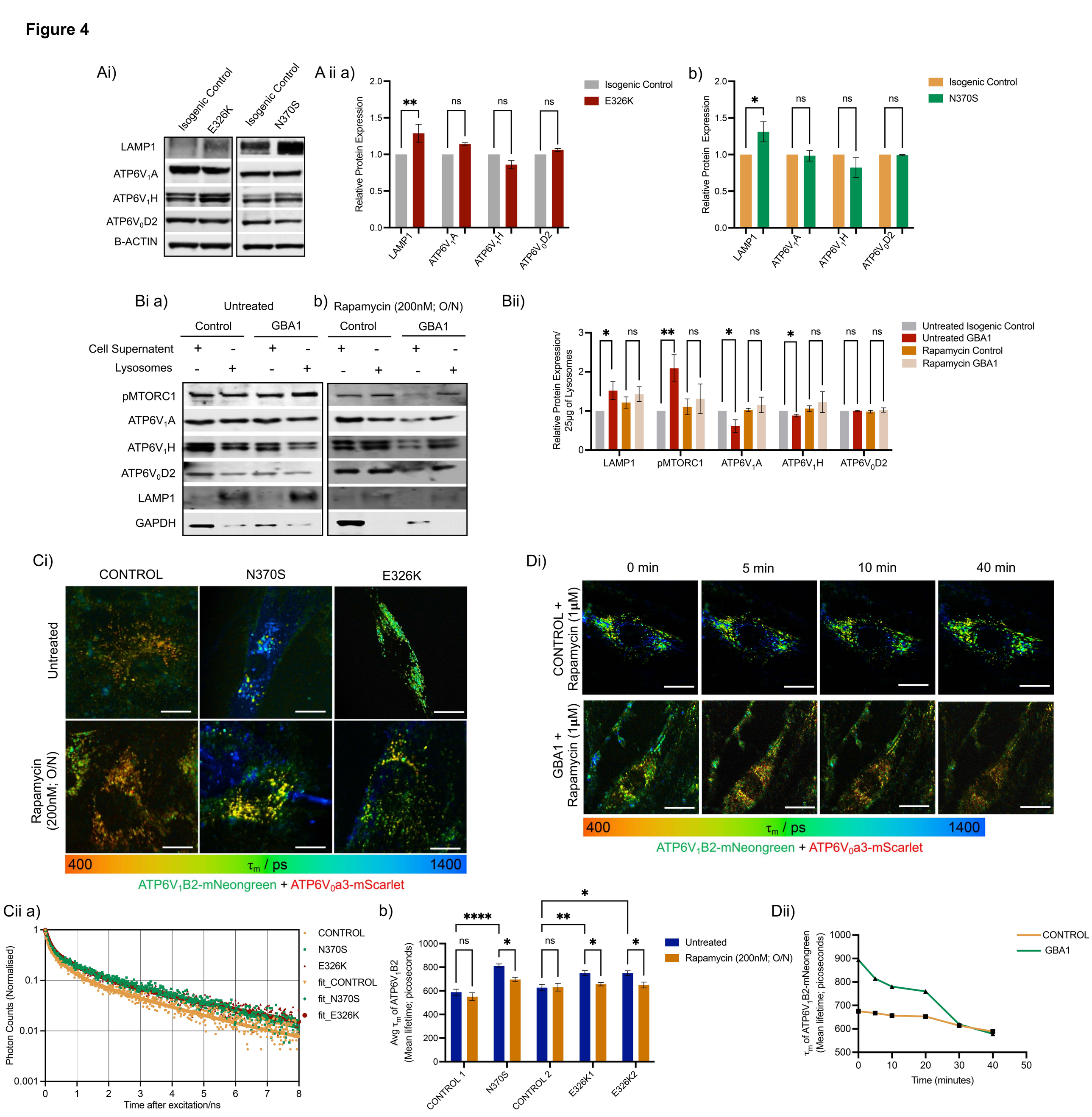
Ai)
Isogenic Control
E326K
Isogenic Control
N370S
LAMP1
ATP6V1A
ATP6V1H
ATP6V0D2
B-ACTIN
A ii a)
Relative Protein Expression
Isogenic Control
E326K
b)
Isogenic Control
N370S
Bi a)
Untreated
b) Rapamycin (200nM; O/N)
Control
GBA1
Cell Supernatent
Lysosomes
pMTORC1
ATP6V1A
ATP6V1H
ATP6V0D2
LAMP1
GAPDH
Bii)
Relative Protein Expression/ 25µg of Lysosomes
Untreated Isogenic Control
Untreated GBA1
Rapamycin Control
Rapamycin GBA1
Ci)
CONTROL
N370S
E326K
Untreated
Rapamycin (200nM; O/N)
400
τm / ps
1400
ATP6V1B2-mNeongreen + ATP6V0a3-mScarlet
Di)
0 min
5 min
10 min
40 min
CONTROL + Rapamycin (1µM)
GBA1 + Rapamycin (1µM)
400
τm / ps
1400
ATP6V1B2-mNeongreen + ATP6V0a3-mScarlet
Cii a)
Photon Counts (Normalised)
Time after excitation/ns
CONTROL
N370S
E326K
fit_CONTROL
fit_N370S
fit_E326K
b)
Avg τm of ATP6V1B2 (Mean lifetime; picoseconds)
Untreated
Rapamycin (200nM; O/N)
CONTROL 1
N370S
CONTROL 2
E326K1
E326K2
Dii)
τm of ATP6V1B2-mNeongreen (Mean lifetime; picoseconds)
Time (minutes)
CONTROL
GBA1

Figure 5

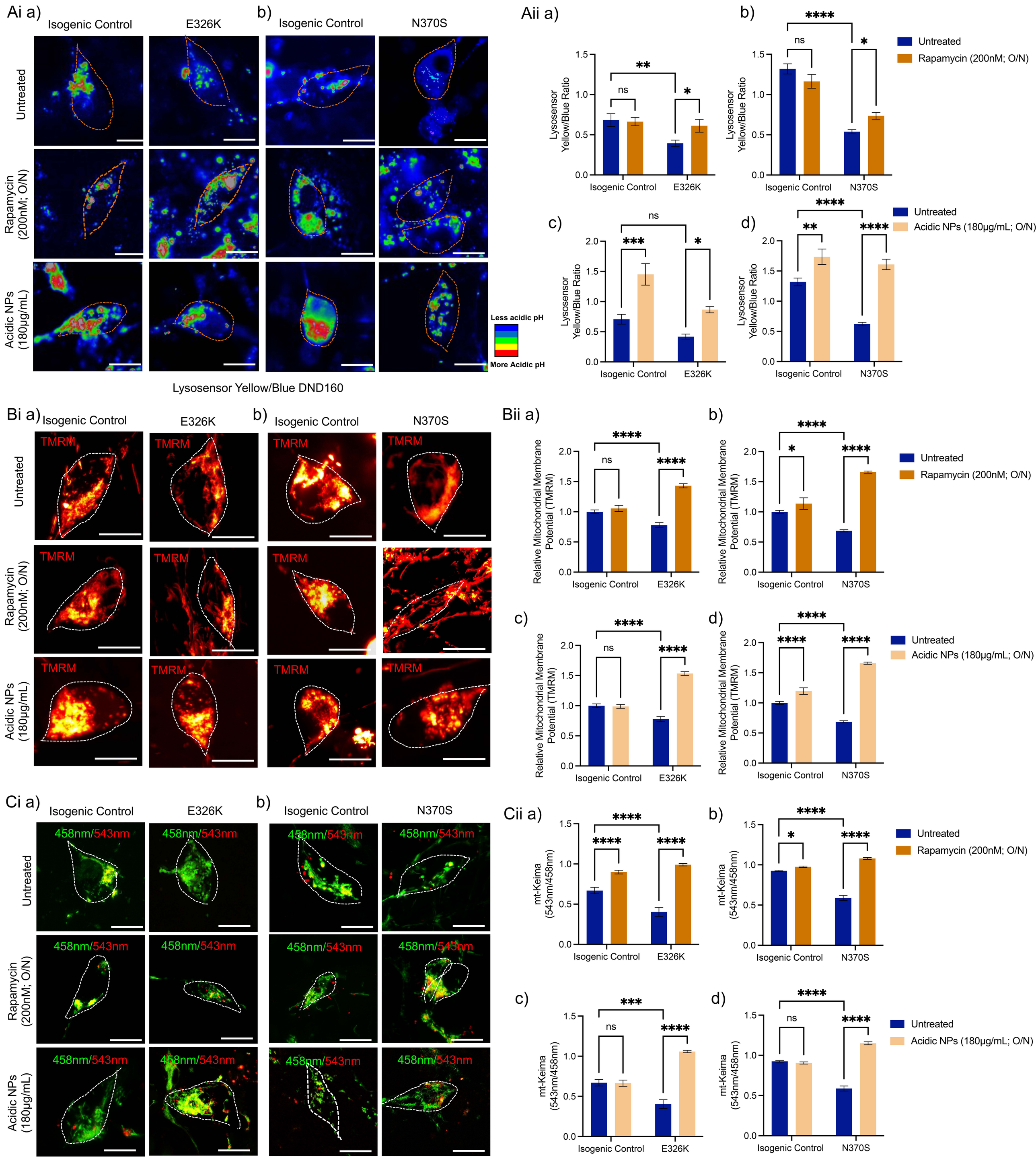
Ai a)
Isogenic Control
E326K
b)
Isogenic Control
N370S
Untreated
Rapamycin (200nM; O/N)
Acidic NPs (180µg/mL)
Less acidic pH
More Acidic pH
Lysosensor Yellow/Blue DND160
Aii a)
b)
c)
d)
Lysosensor Yellow/Blue Ratio
Untreated
Rapamycin (200nM; O/N)
Acidic NPs (180µg/mL; O/N)
Isogenic Control
E326K
N370S
Bi a)
TMRM
Bii a)
Relative Mitochondrial Membrane Potential (TMRM)
Ci a)
458nm/543nm
Cii a)
mt-Keima (543nm/458nm)

Figure 6

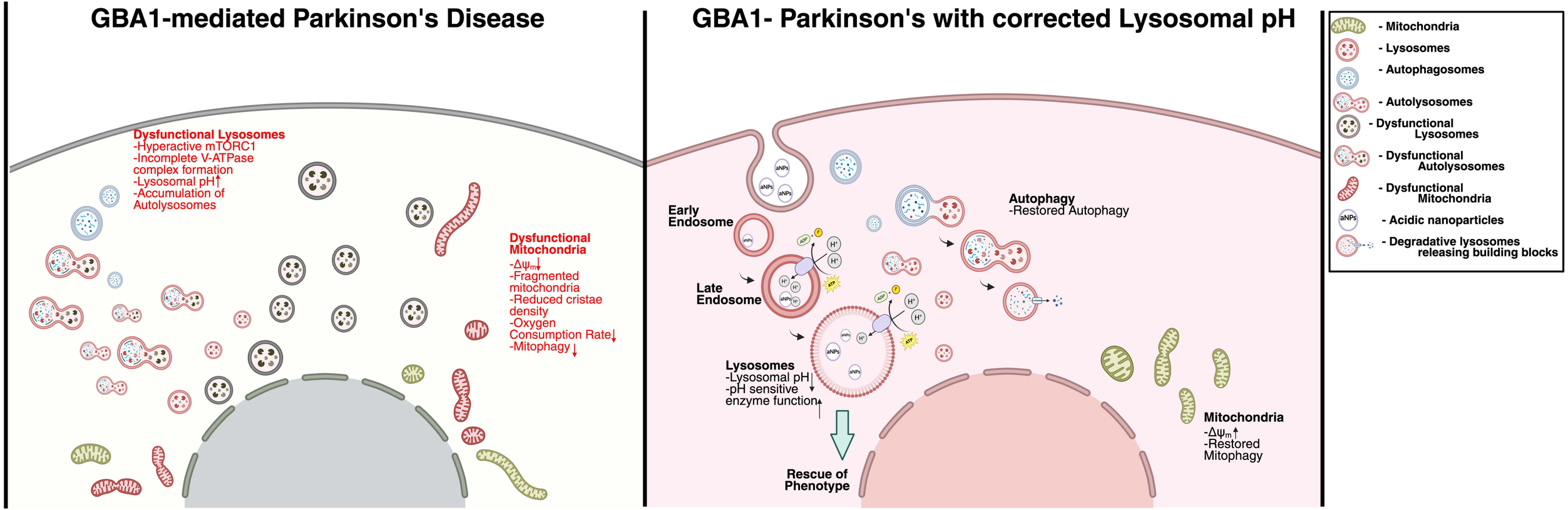
GBA1-mediated Parkinson's Disease
Dysfunctional Lysosomes
-Hyperactive mTORC1
-Incomplete V-ATPase complex formation
-Lysosomal pH↑
-Accumulation of Autolysosomes
Dysfunctional Mitochondria
-Δψm↓
-Fragmented mitochondria
-Reduced cristae density
-Oxygen Consumption Rate↓
-Mitophagy↓
GBA1- Parkinson's with corrected Lysosomal pH
Early Endosome
Late Endosome
Lysosomes
-Lysosomal pH↓
-pH sensitive enzyme function↑
Rescue of Phenotype
Autophagy
-Restored Autophagy
Mitochondria
-Δψm↑
-Restored Mitophagy
- Mitochondria
- Lysosomes
- Autophagosomes
- Autolysosomes
- Dysfunctional Lysosomes
- Dysfunctional Autolysosomes
- Dysfunctional Mitochondria
- Acidic nanoparticles
- Degradative lysosomes releasing building blocks

Supplementary Figure 1

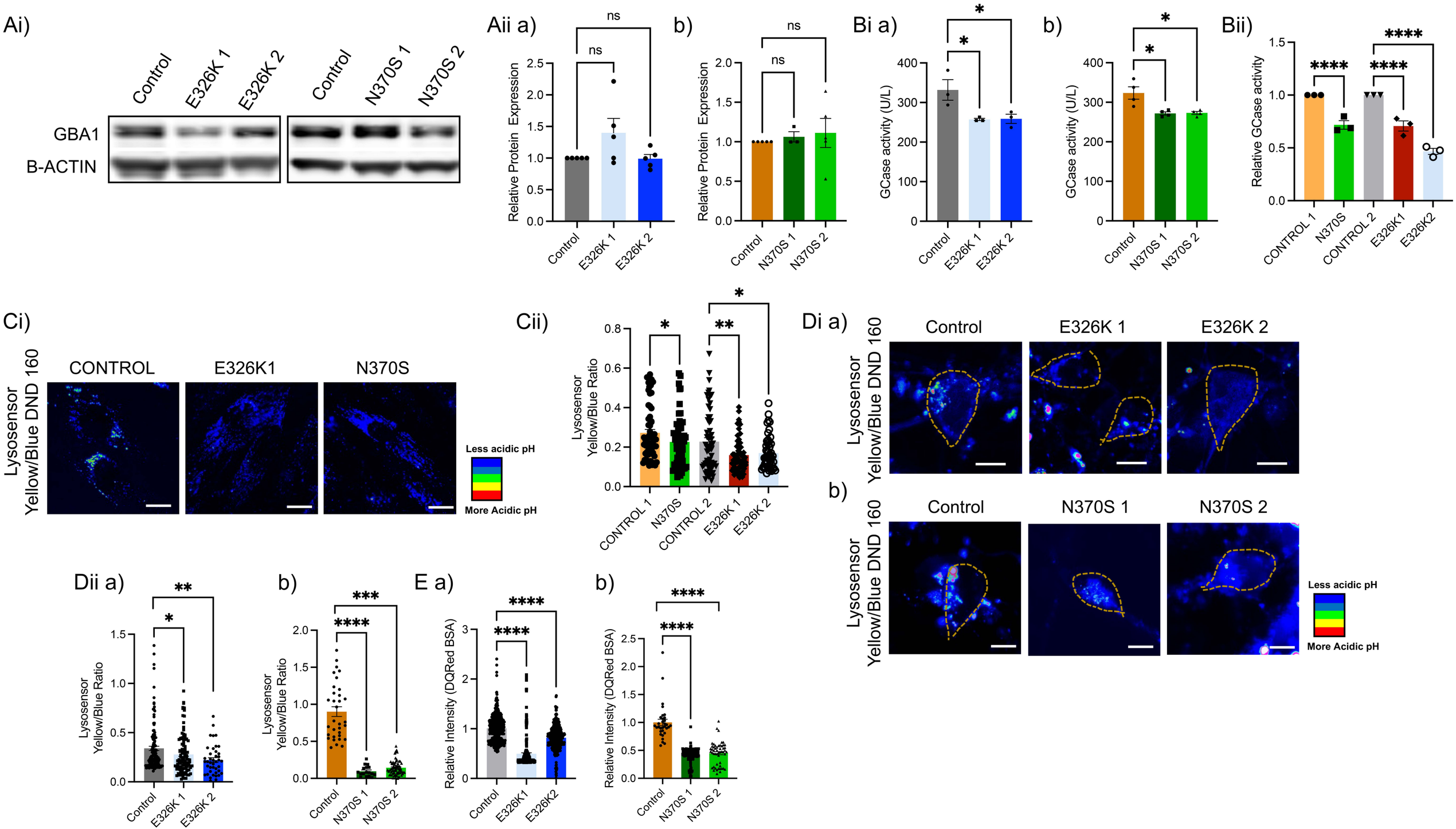

Supplementary Figure 2

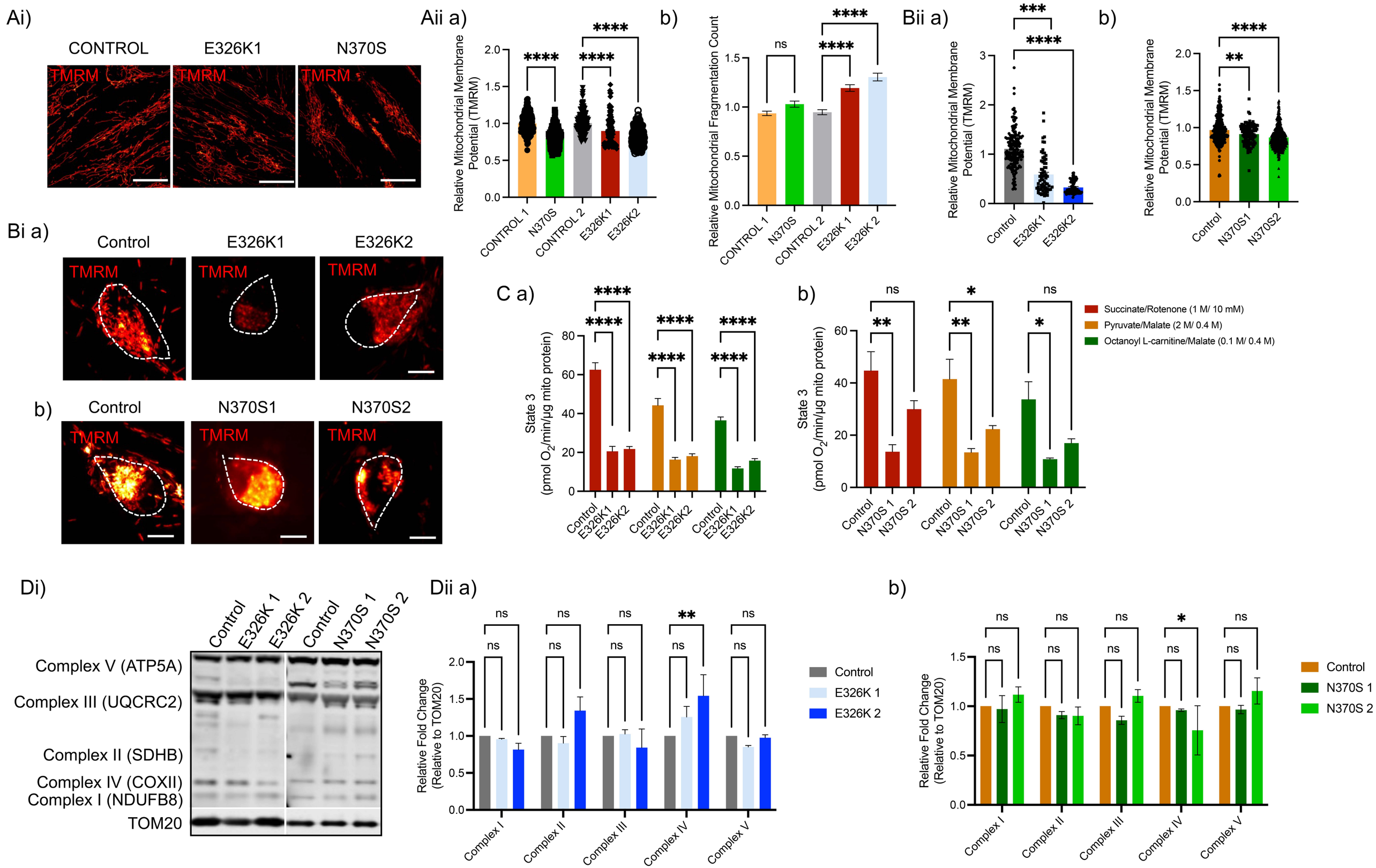

Supplementary Figure 3

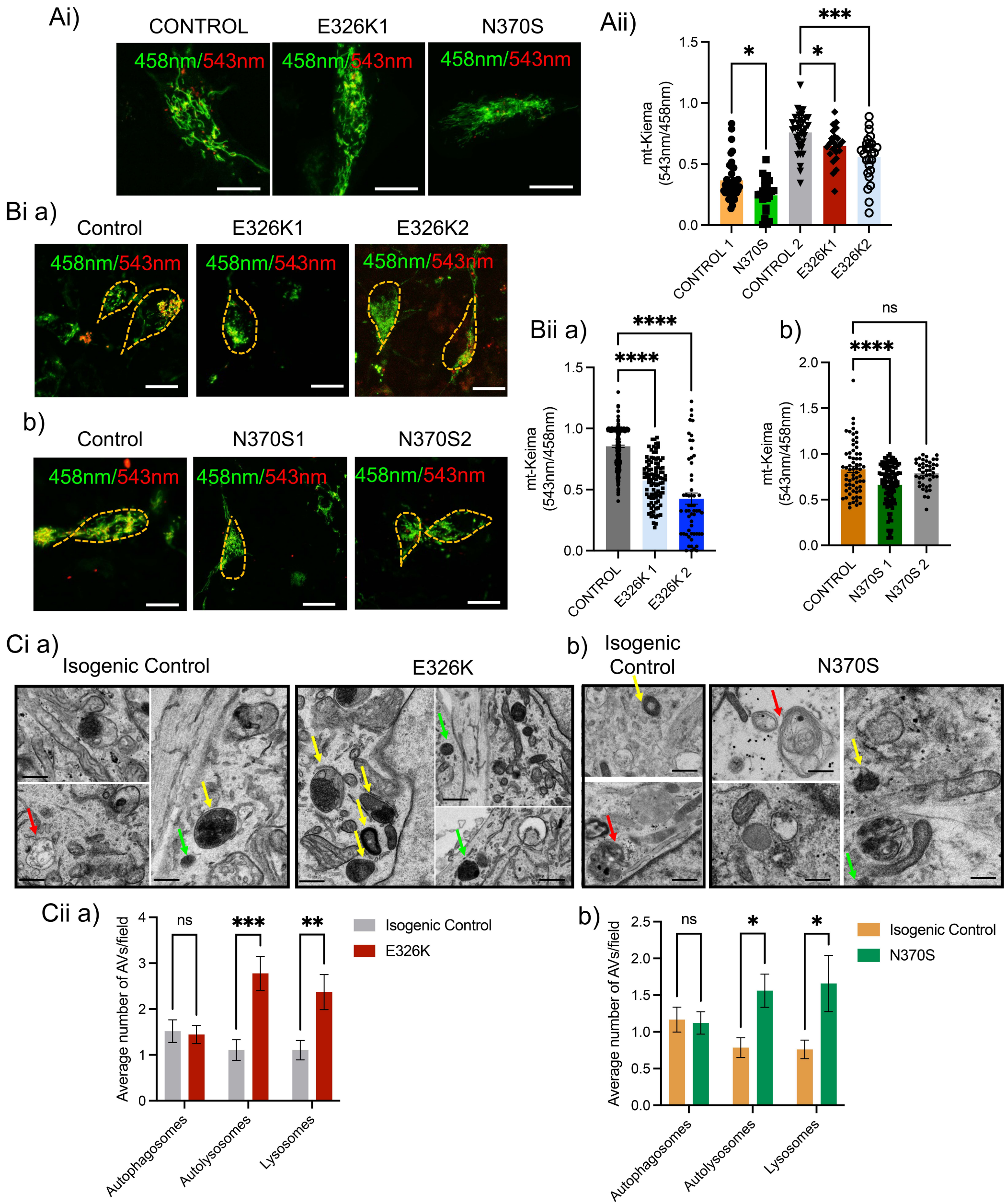
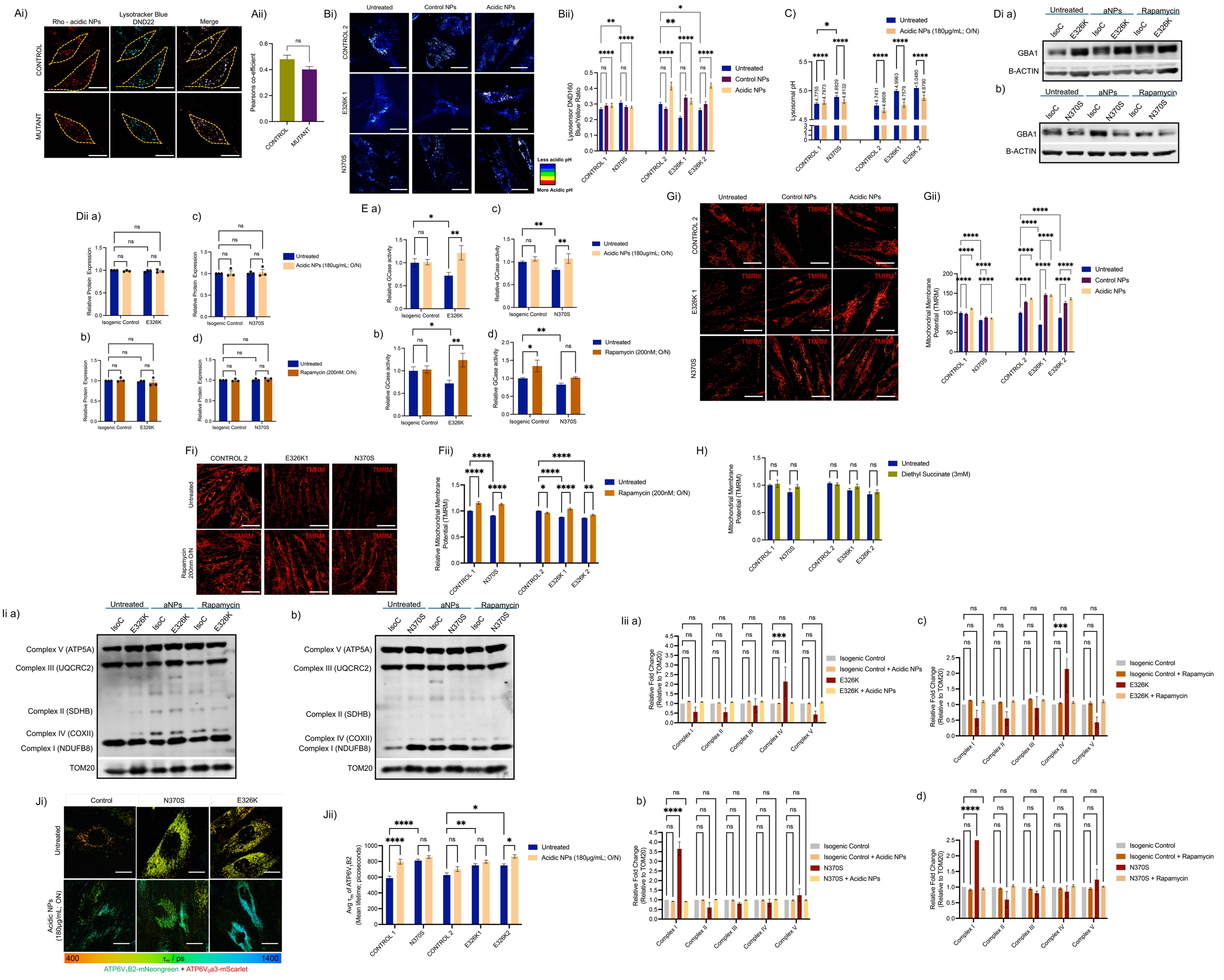
Supplementary Figure 4